This is a previous version of the article published in Journal of Catalysis. 2016, 338: 154-167. doi:10.1016/j.jcat.2016.03.004

One step-synthesis of highly dispersed iron species into silica for propylene epoxidation with dioxygen

J. García-Aguilar[a], *I. Miguel-García*[a], *J. Juan-Juan*[b], *I. Such-Basáñez*[b], *E. San Fabián*[c], *D. Cazorla-Amorós*[a], *Á. Berenguer-Murcia*[a,*].

[a] Materials Science Institute and Inorganic Chemistry Department, Alicante University, Ap. 99, E-03080 Alicante, Spain.

[b] Research Technical Services, Alicante University, Ap. 99, E-03080 Alicante, Spain.

[c] Materials Science Institute and Physical Chemistry Department, Alicante University, Ap. 99, E-03080 Alicante, Spain.

Keywords: propylene, epoxidation, ferrosilicate, dioxygen, DFT.

ABSTRACT: Well dispersed iron catalysts were synthesized in silica ($Fe_{0.0X}SiO_2$) by a one-step synthesis procedure. These materials were tested in the propylene epoxidation reaction with gaseous O_2. The influence of the iron metal loading on the iron incorporation and distribution in the support (both influenced by the synthetic procedure) were thoroughly studied (conversion, generation and selectivity). Electron Microscopy and UltraViolet-Visible (UV-VIS), Raman and Fourier Transform Infrared Spectroscopy (FTIR) spectroscopy techniques were used to analyze the iron distribution in the catalysts and to probe its incorporation into the silica framework. In-situ FTIR was also used to analyze the interaction between propylene and iron-based catalysts.

Computational calculations considering a single-site iron catalyst incorporated into the silica structure show a possible interaction between O_2 and the incorporated iron atom and the olefin bond and the acidic proton neighboring the iron species which favours the reaction between the two molecules near the iron atom.

1. Introduction

In the last years, the fine chemicals industry is facing an important challenge concerning the production of one important intermediate in the synthesis of polyurethanes, cosmetics, solvents, detergents and other relevant products. This new attractive compound is propylene oxide (PO) and its properties and reactivity make this product one of the most widely studied, not only by academic researchers, but also by the main chemicals manufacturers, such as DOW Chemical and LyondellBasell Industries [1]. PO is principally consumed in the production of polyether polyols for urethanes (65%) and the synthesis of propylene glycols (19%) and glycol ethers (6%), these compounds being synthesized by oligomerization, hydration and alcoholysis of raw PO, respectively [2].

In the industrial scale synthesis of PO, propylene is used as raw material. In this sense, approximately 7% of the world consumption of propylene is for PO production, representing the third product generated from this precursor, only behind polypropylene (62%) and acrylonitrile (8%) [2]. Nowadays, the main PO production route is the liquid-phase reaction, known as chlorohydrin process, with approximately 50% of PO production. Other liquid-phase PO production processes employed in industry nowadays include the styrene co-product process (33% PO production worldwide), the tert-butyl co-product process (15%), the HPPO (hydrogen peroxide-based) process (5%), and the Sumitomo cumene-based process (5%). Some problems

associated with these syntheses are the use of chlorine and sub-production of chlorinated organic compounds in the reaction that result in a complicated separation and purification of PO [3].

In this sense, propylene epoxidation to propylene oxide by gas-solid phase heterogeneous catalysis could avoid the use of hazardous oxidation agents such as Cl_2, in the liquid phase and replace them with other safer compounds, such as H_2/O_2 mixtures or O_2 in the best case scenario [2,4]. In the literature, the most common and widely developed catalysts for this process are based in titano-silicate supports (Ti-SiO_2) with well dispersed Au nanoparticles on the surface of the material. This kind of materials presents very well dispersed Ti(IV) species on the silica matrix, generally with low Ti/Si ratios. In these cases, the chemical properties of the Ti-SiO_2 reflect in an enhanced performance of the active phase in the epoxidation process compared to the behavior of pure TiO_2-based catalysts, both in terms of activity and selectivity for the process [5,6].

Moreover, the deposition of low metal loadings of Au as nanoparticles (less than 5 nm in size) drastically increases the selectivity (over 90% towards PO) at temperatures above 100-200ºC. These catalysts have been widely studied and nowadays the reaction mechanism for this active phase is well known, with the formation of hydroperoxo and peroxo species on the metal nanoparticles and their interaction with propylene molecules adsorbed on titanium sites [7] being responsible for the high selectivity towards PO.

These catalysts have been developed in microreactor configurations [8] and membrane reactors [9]. However, the use of H_2/O_2 mixtures in the gas stream is mandatory to achieve an acceptable selectivity towards PO. In this sense, many works have demonstrated the validation of these supports, by modifying the silica support, the titanium precursor and the Au nanoparticles deposition method. Nevertheless, some aspects such as low propylene conversion, water

formation and the low H_2 efficiency are the main drawbacks of this active phase and still need to be overcome. Recently, some authors have tested this kind of gold-based catalysts (Au/TiO_2) in a different oxidative atmosphere (CO/O_2) with comparable results (in terms of propylene conversion and PO selectivity) to those reached under a H_2/O_2 gas stream composition [10]. Ag nanoparticles have been also supported on TiO_2, but poorer results have been obtained compared to the gold-based catalysts, yielding lower propylene conversions [11]. Also, similar catalysts such as $Ti\text{-}SiO_2$ loaded with Pt or Pd nanoparticles have been tested in the epoxidation of propylene in liquid phase by in-situ generation of H_2O_2 adding H_2 and O_2 in the organic phase [12].

On the other hand, the use of a gas stream with O_2 as oxidative agent, without the addition of H_2, is employed in some catalysts for the synthesis of PO by epoxidation of propylene. Ag-based catalysts on different supports (such as $CaCO_3$, Al_2O_3, MoO_3/ZrO_2 and WO_3) [3,13], have been studied in the epoxidation of propylene with O_2 between 250-350ºC. The catalytic behavior of these materials shows lower selectivity than the $Au/Ti\text{-}SiO_2$ systems in H_2/O_2 gas streams compositions but with a similar propylene conversion [14]. In other related works, the catalysts studied for the propylene epoxidation reaction are based on different metal oxides (Ru and/or Cu) [15–17] also tested in O_2-containing atmospheres. In these cases, a PO selectivity of 35% and 9% propylene conversion is achieved for a 2% Cu-5% Ru-1.75% NaCl promoted catalyst supported over silica at 350ºC. Also, mixed copper/manganese oxides promoted with NaCl at 300ºC, have displayed propylene conversions around 5% and PO selectivities of 25% [18]. Other works use more complicated systems to achieve good catalytic behaviors, such as $Ti\text{-}MoO_3\text{-}Bi_2SiO_5/SiO_2$, that displays 20% of propylene conversion and 60% of PO selectivity at 500ºC [19].

Some works have studied iron impregnated or incorporated in silica as active phase for selective hydrocarbon oxidations. In this sense, the iron location (framework or extra-framework), iron coordination (tetrahedral or octahedral) or its distribution (single-sites, clusters or small particles) are the main factors discussed for the selective oxidation but, in all cases, the iron has been stated to produce the decomposition of the oxidizing agent (H_2O_2 or N_2O) and the resulting adsorbed atomic oxygen has been identified as the species responsible for the oxidation. As an example, the activation of N_2O for the oxidation of benzene to phenol requires of extra-framework iron species in Fe-MFI catalyst [20]. In the epoxidation of styrene with H_2O_2, two different species of iron have been found to be important for the oxidation reaction, i.e., iron oxide clusters are responsible for the H_2O_2 decomposition and tetrahedral iron in framework positions are the sites where the epoxidation effectively takes place [21]. This kind of well-dispersed iron-based catalysts has been also used for selective oxidations in other liquid phase processes, with very successful results [22,23].

In the propylene epoxidation reaction using iron-based catalysts, the use of a more oxidant compound, such as N_2O at 350ºC, is necessary for the PO synthesis in the gas-phase reaction [24–27]. E. Ananieva et al. studied the effect of Na^+ and Cs^+ in the acidity of the support to decrease the possibility of PO polymerization [24]. In addition, B. Horváth et al. focused their work on the addition of the alkaline promotor K^+ (as KCl) in order to enhance the catalytic properties of the iron containing catalyst. Maximum PO selectivity during the catalytic tests was achieved (around 75%) for a KCl promoted iron impregnated silica, but deactivation of the catalyst was observed due to carbon deposition on the catalyst, even when the promoting agent was added. In this sense, the authors propose that the epoxidation reaction takes place *via* the oxygen-atoms abstracted from the N_2O which decomposes in the medium. The specific iron

species responsible for the N_2O decomposition could transfer the oxygen atoms and react with propylene, generating PO [25]. Most of these related, promoted or unpromoted, catalyst used in propylene epoxidation reaction have been prepared using multiple-step procedures (e.g. support preparation and/or metal impregnation).

In this work, we present a one-step synthesis method for the preparation of Fe-SiO_2 catalysts, with very well dispersed iron species into the silica structure, and their application in the propylene epoxidation reaction using only the O_2 molecule as oxidant. The comparison between samples with different preparation procedures (one-step synthesis and impregnation) and their characterization by different spectroscopic (UV-VIS, Raman and FTIR), microscopy (TEM and FE-SEM) techniques and complementary simulation calculations (dispersion-corrected DFT) allows obtaining information about the reaction mechanism for the epoxidation reaction investigated on the postulated iron species incorporated into the silica structure.

2. Experimental

2.1 Catalyst Preparation

2.1.1 Preparation of the $Fe_{0.0X}SiO_2$ Catalysts (One-step synthesis)

The mesoporous Fe-doped silica catalysts have been prepared adapting a sol-gel synthetic protocol described for pure SiO_2 in other works [28,29].

In a typical synthesis, 0.400 g of surfactant (Pluronic® F127, BASF), 0.452 g of urea (Sigma-Aldrich) and 5.052 g of 0.01M acetic acid solution were mixed under vigorous stirring for 80 min, the final pH of the resulting solution being around 4. Then, the necessary amount of iron

precursor (iron (III) nitrate nonahydrate, $Fe(NO_3)_3 \cdot 9H_2O$, 99.99%, Sigma-Aldrich) is added in the solution and the mixture is stirred for 1 h. Subsequently, the solution was cooled in an ice-water bath maintaining the stirring and the silica precursor was added dropwise (2.030 g Tetramethyl orthosilicate, TMOS, Sigma-Aldrich). This solution was kept under stirring for 40 min at 0ºC.

Finally, the sol was introduced in a Teflon autoclave and heated at 40ºC for 20 h to produce the aging of the sol (the pH after this step remained around 4). After this, the sample is submitted to a hydrothermal treatment at 120ºC for 6 h, to produce the urea decomposition (the final pH of the supernatant liquid being around 9-10). After this step, a dark supernatant liquid phase is observed for samples with a Fe/Si ratio over 0.01, which was removed from the top of the monolith generated, corresponding to the excess of Fe not incorporated in the SiO_2 structure. As a final step, the monolith is calcined at 550ºC for 6 h to eliminate the surfactant and the rest of unwanted precursors.

Four samples with different Fe/Si molar ratios have been prepared (namely 0.005, 0.01, 0.02 and 0.03). Higher Fe content cannot be incorporated in these structures, since high amounts of $Fe(NO_3)_3$ in the initial sol lead to mechanical instability of the active phase (a sample prepared with a 5% iron molar ratio content crumbled during the thermal calcination of the material) and the mixed oxide cannot be generated. The samples in this work have been named according to the nominal Fe/Si molar ratio in each case, for example $Fe_{0.01}SiO_2$ corresponds to the sample with 1 mol % Fe in the oxide (with respect to Si moles). The samples prepared by this procedure are all white in color, except for the one with a higher Fe content (Fe/Si=0.03) which is brown.

2.1.2 Preparation of the Fe impregnated-SiO_2 Catalyst

For comparison purposes, an iron-based silica catalyst has been prepared by wet impregnation. For that, 300 mg of pure mesoporous silica (prepared by the aforementioned procedure without the iron precursor) and the necessary amount of $Fe(NO_3)_3 \cdot 9H_2O$ to yield a metal loading of 1 mol % Fe were stirred in water for 2 days. Then, the solvent was evaporated under stirring by heating the suspension at 80ºC, keeping the magnetic stirring until complete evaporation of the solvent. Finally, the powder was calcined in an oven at 550ºC for 6 h, and the sample was labeled as $Fe_{impreg}SiO_2$.

2.2 Characterization

All the prepared catalysts have been analyzed by Field Emission Scanning Electron Microscopy (FE-SEM, Merlin VP Zeiss) before the catalytic tests to determine the morphology of the samples and how the metal incorporation reflects in the silica texture. The samples were also characterized by Transmission Electron Microscopy (TEM) coupled to Energy Dispersive X-Ray Analysis (EDX) with a JEOL JEM-2010 microscope operating at 200 kV with a space resolution of 0.24 nm. For the analysis, a small amount of the sample was suspended in a few drops of ethanol, and sonicated for a few minutes. A drop of this suspension was then deposited onto a 300 mesh Lacey copper grid and left to dry at room temperature. TEM analyses allowed the evaluation of the metal incorporation, the formation of small particles of iron and the quantification of the metal loading by the coupled EDX.

Spectroscopic techniques were also used for characterization purposes. The prepared materials were analyzed using a UltraViolet-Visible-Near-Infrared (UV-VIS-NIR, V-670, JASCO) equipped with a double monochromator system, a photomultiplier tube detector and an integrating sphere (ISN-723 UV-Visible-NIR, JASCO) which enables the possibility to measure

the diffuse reflectance or diffuse transmittance of a solid powder. The catalysts have been analyzed before and after the catalytic tests. *In-situ* Fourier Transform Infrared Spectroscopy (FTIR, FTIR-4100, JASCO) was also used for the study of the solid-gas reaction in the different catalysts. FTIR spectra were collected in the single beam mode at different times while a gas stream of: 10 vol. % C_3H_6/He, 10 vol. % O_2/He or the reaction gas stream composition (10% C_3H_6, 10% O_2/He) is flowed through the sample for at least 5 minutes to ensure whichever interaction between the catalysts and the propylene. Afterwards, the gas stream was shifted to pure He and the evolution of the spectra corresponding to the catalyst surface was also studied by FTIR. Spectra were collected at different temperatures (150, 250 and 350ºC) and with an interval time of 15 seconds. The results have been presented by subtracting the spectrum corresponding to the pure catalyst to that obtained at the same temperature. Furthermore, this technique has been also used to analyze the incorporation of the iron into the silica framework studying the modification of the vibrational bonds of the silica and the iron based silica in the fresh catalyst after their dry at 120ºC for 24h. UV-Raman (NRS-5100, Jasco) has been used to analyze the incorporation of iron into the silica framework. The catalysts have been irradiated for 30 minutes with a UV lamp (HeCd, 325 nm, 1 mW). The equipment is equipped with a Thorlabs 20x UV objective.

The iron metal loading of the catalysts was analyzed by inductively coupled plasma-optical emission spectroscopy (ICP-OES), in a Perkin-Elmer Optima 4300 system. The necessary amount of sample was dissolved in 0.1 ml of HF (5 vol. %) at room temperature, in order to ensure the total dissolution of the samples, and then diluted to the linear iron detection range (0.05-10 ppm).

The iron based catalysts were also characterized by N_2 adsorption−desorption measurements at −196°C (Quantachrome, Autosorb 6B) to analyze the porous texture of the catalysts.

2.3 Propylene Epoxidation Tests

The samples were first tested under non-isothermal conditions at a heating rate of 3ºC/min up to 450ºC to analyze the catalytic performance of the samples. Once the non-isothermal reactions were performed, the temperature for the isothermal reaction was chosen and the behaviour of the catalysts was tested for at least 4 hours at ambient pressure under steady-state conditions. At the conditions chosen (350ºC), low propylene conversion and high PO selectivity were obtained.

In all cases, the propylene epoxidation was evaluated using 200 mg of powder catalyst introduced in a quartz reactor, and the gas stream was maintained constant to obtain a WHSV of 10000 $ml \cdot g^{-1} \cdot h^{-1}$ (STP), with a gas composition of 10% C_3H_6, 10% O_2, 80% He. When several catalytic cycles were performed for a sample, the catalysts were treated at 550ºC in synthetic air between cycles to ensure the total elimination of any carbonaceous deposit that could be formed during the former catalytic test.

The gas composition of the reaction was analyzed with a GC chromatograph (Agilent 7820A) equipped with two columns, PoraBond Q (Agilent) and CTR-I (Alltech), for the separation of the organic (propylene, propane, propylene oxide, acetaldehyde, acetone) and the inorganic (O_2 and CO_2 mainly) compounds respectively. The main possible organic by-products have been analysed separately. Calibration for was performed introducing each pure compound separately in a quartz reactor at a controlled temperature (accuracy ± 0.1ºC) to obtain the desired range of partial pressure. A constant flow of He (30 ml/min of He) was passed through the reactor and the resulting stream was analyzed in the GC. Their respective retention times are shown in the

Supplementary Information (Fig. S1), with the GC analysis of the most and the least selective catalyst, $Fe_{0.005}SiO_2$ and $Fe_{0.03}SiO_2$ respectively as examples of the analysis done. Inorganic by-products include CO_2 and H_2O. Propylene conversion, PO generation and PO selectivity, all of them as percentage, are calculated using the following equations and with the respective calibration for each compound in order to describe the catalytic behaviour of the samples. TOF, calculated from the moles of PO generated per hour per mole of Fe contained in the catalyst (and quantitatively determined by ICP-OES) has been used to assess the catalytic performance of the samples. Given the inherent difficulty in differentiating between the well-dispersed iron species (present as single or di-iron sites) and larger iron species present in the catalyst (mainly forming small oxide particles), this approach was taken as a simple and illustrative way to present and compare our results.

$$Propylene\ Conversion\ \ \% \ = \frac{C_{C_3H_6-in} - C_{C_3H_6-out}}{C_{C_3H_6-in}} \times 100$$

$$PO\ Generation\ \ \% \ = \frac{C_{PO-out}}{C_{C_3H_6-in}} \times 100$$

$$PO\ Selectivity\ \ \% \ = \frac{C_{PO-out}}{C_{C_3H_6-in} - C_{C_3H_6-out}} \times 100$$

2.4 Computational calculations

The energy calculations and geometry optimizations were performed with Gaussian09 program [30], using the hybrid non-local B3LYP method [31,32] and the 6-31G(d,p) basis set for all atoms [33–35].

The dispersion energies were considered using the D3(BJ) method [36,37] in all calculations.

The zero-point vibrational energies (ZPE) obtained were scaled according to Wong (0.9804) [38]. The basis set superposition error (BSSE) was calculated and taken into account using the Counterpoise Theory for the base pair complex energies [39,40]. Visualization of the structures was performed using Avogadro 1.1 software [41]. Ferrosilicate structure was modelled using the FeH19O7Si7 cluster, which had been previously used to simulate acidic catalytic performance on Fe-MFI [42].

Three different adsorbate-cluster complex structures were considered. One formed by dioxygen and the ferrosilicate cluster, and the other two formed by propylene approaching the ferrosilicate cluster in two different ways. A full optimization of the complex geometry was carried out, obtaining vibrational information in the calculation and no imaginary frequencies were observed in any of the situations presented in this work. In the cluster and the complex, we have considered several possible spin multiplicities, whereas the adsorbates have their ground state multiplicities: singlet in the case of propylene and triplet in the case of oxygen.

Interaction energies between adsorbate and the cluster model were calculated by the following formula

$$E_{int} = - E_{complex} - E_{cluster} + E_{adsorbate}$$

where E_{int} is the interaction energy between adsorbate and the cluster model, $E_{cluster}$ is the energy of the cluster maintaining the structure of the adsorbent-cluster complex, $E_{adsorbate}$ is the energy of the optimized adsorbate and $E_{complex}$ is the energy of the optimized adsorption complex (adsorbate-cluster complex).

3. Results and discussion

3.1 Morphological and Chemical Analysis of the Catalysts

ICP-OES analysis served to establish the Fe content in each catalyst. The results indicated that the Fe content is very close to the one targeted in each synthesis, with the incorporation of approximately 93% of the desired Fe in the final SiO_2 structure in all cases. In this sense, the obtained Fe/Si ratio is 0.00428 ± 0.00005, 0.00952 ± 0.00005, 0.0186 ± 0.0003 and 0.0288 ± 0.0002 for the samples with nominal contents of 0.005, 0.01, 0.02 and 0.03, respectively. For the impregnated sample, the iron content has been determined to be 0.0099 ± 0.0001, which is also very close to the targeted 0.01 Fe/Si ratio. It should be mentioned that for the sol-gel Fe-based catalysts, complete incorporation of the Fe into the SiO_2 structure did not take place, as described in the Experimental Section (Section 2.1.1), since a dark supernatant liquid phase was observed covering the generated SiO_2 monolith and removed before the calcination step.

All the samples prepared in this work have been analyzed by N_2 and CO_2 adsorption and no significant changes have been observed between the pure silica and the different catalysts. In all cases, the catalysts show a combination of type I and type IV isotherms typical of predominantly mesoporous materials (see Fig. S2 in Supplementary Information) with a slight microporous contribution. The materials also show a certain degree of macroporosity due to the interparticle gap between the silica spheres and microporosity inherent to materials formed by precipitated silica [43]. The specific surface area of the samples calculated by the BET method is around ~230 m^2/g in all cases, with a mesopore size distribution from 5 to 20 nm according to the BJH model applied to the desorption branch of the N_2 isotherms. The obtained silica has a low micropore volume of 0.09 cm^3/g calculated by the Dubinin−Radushkevich method in N_2 adsorption.

The catalysts were observed by FE-SEM in order to evaluate the morphological appearance of the prepared powders. The micrographs are shown in Fig. 1 and it can be observed that, due to

the synthetic procedure, the pure silica synthesized in this work is generated in the form of spheres with a very well defined morphology (Fig. 1A), with the silica particles size being around 3-6 μm in diameter, as previously reported in other works [28,29]. As it can be observed, the incorporation of low loadings of Fe in the SiO_2 structure may reflect in significant modifications of the particles morphology. For the samples $Fe_{0.005}SiO_2$ and $Fe_{0.01}SiO_2$ (Fig. 1B and 1C), the spherical shape of the catalysts can be observed, although a slight distortion of the spheres is obtained. In the samples with higher metal loadings, ($Fe_{0.02}SiO_2$ and $Fe_{0.03}SiO_2$), the samples show a very different morphology and the spheres cannot be appreciated in the images. Instead, a shapeless continuous material with high surface roughness is obtained (Fig. 1D and 1E).

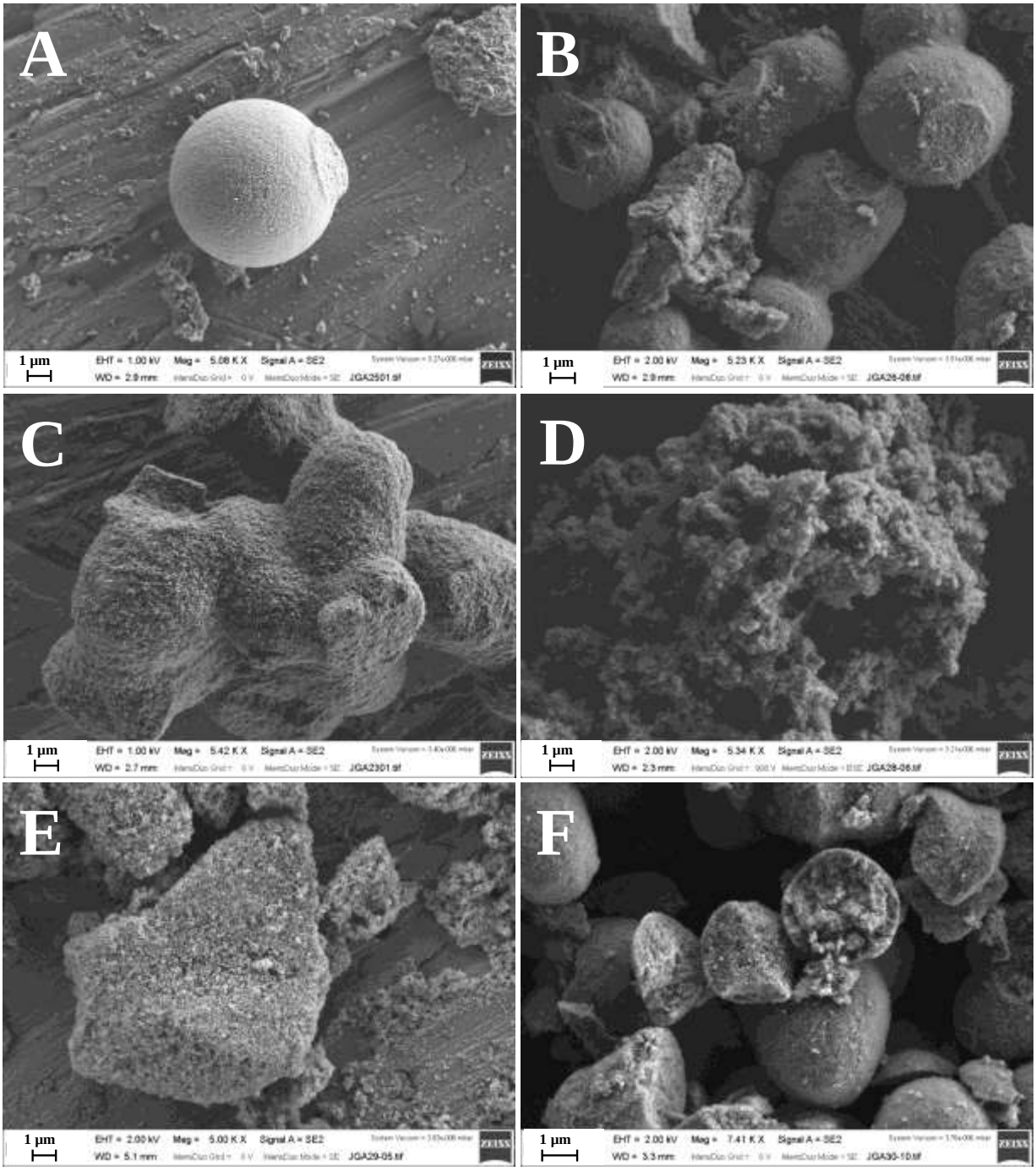

Fig. 1. Field Emission Scanning Electron Microscopy (FE-SEM) of the fresh samples prepared in this work. Samples; A) SiO_2, B) $Fe_{0.005}SiO_2$, C) $Fe_{0.01}SiO_2$, D) $Fe_{0.02}SiO_2$, E) $Fe_{0.03}SiO_2$ and F) $Fe_{impreg}SiO_2$.

In this sense and according to our results, low iron loadings could be incorporated efficiently in the silica structure while maintaining the morphology of the solid, indicating that the Fe atoms might be very well dispersed in the SiO_2 structure. On the other hand, it seems that Fe contents above 2 mol % are too high to efficiently incorporate into the silica structure without distortion, and therefore yield SiO_2–based materials with a very different morphology, as it can be observed in the micrographs.

The formation mechanism of the silica spheres is a very well-known process described in the literature, consisting of a hydrothermal treatment in an autoclave (at 120ºC during 6 h) and subsequent urea decomposition, forming NH_3 and increasing the pH of the solution/gel up to 10. The high pH in the reaction medium, together with the temperature and pressure produce the spinodal decomposition of the aqueous and silica phases and the solution/precipitation reactions of the silica take place, forming the SiO_2 μ-spheres [28,29]. When the iron precursor is added to the synthesis solution, the iron can interact with the silicate species during the sol/gel process and precipitate together with the SiO_2 phase. In this sense, if the Fe content is too high (above 2 mol % in this work) not all the iron can be incorporated appropriately in the structure and therefore the spherical morphology cannot be obtained, as previously mentioned.

For the impregnated catalyst (Fig. 1F), spherical particles of SiO_2 of similar size have been detected. However, in this case, a significant fraction of the SiO_2 spheres was fractured, probably due to the impact of said spheres with the stirring bar during impregnation (48h under stirring) which contrasts with the spherical particles found for pure-silica synthesized by a one-step sol-gel process).

For these catalysts, no large particles of iron oxide can be observed on the catalyst surface. However, in all cases, Fe is detected by EDX (Fig. S3 top) and ICP. For the $Fe_{0.005}SiO_2$ catalyst, the Fe, Si and O distribution obtained by elemental mapping are shown in Fig. S4, where no Fe agglomeration is observed in the sample.

Transmission electron microscopy images of the catalysts are presented in Fig. 2.

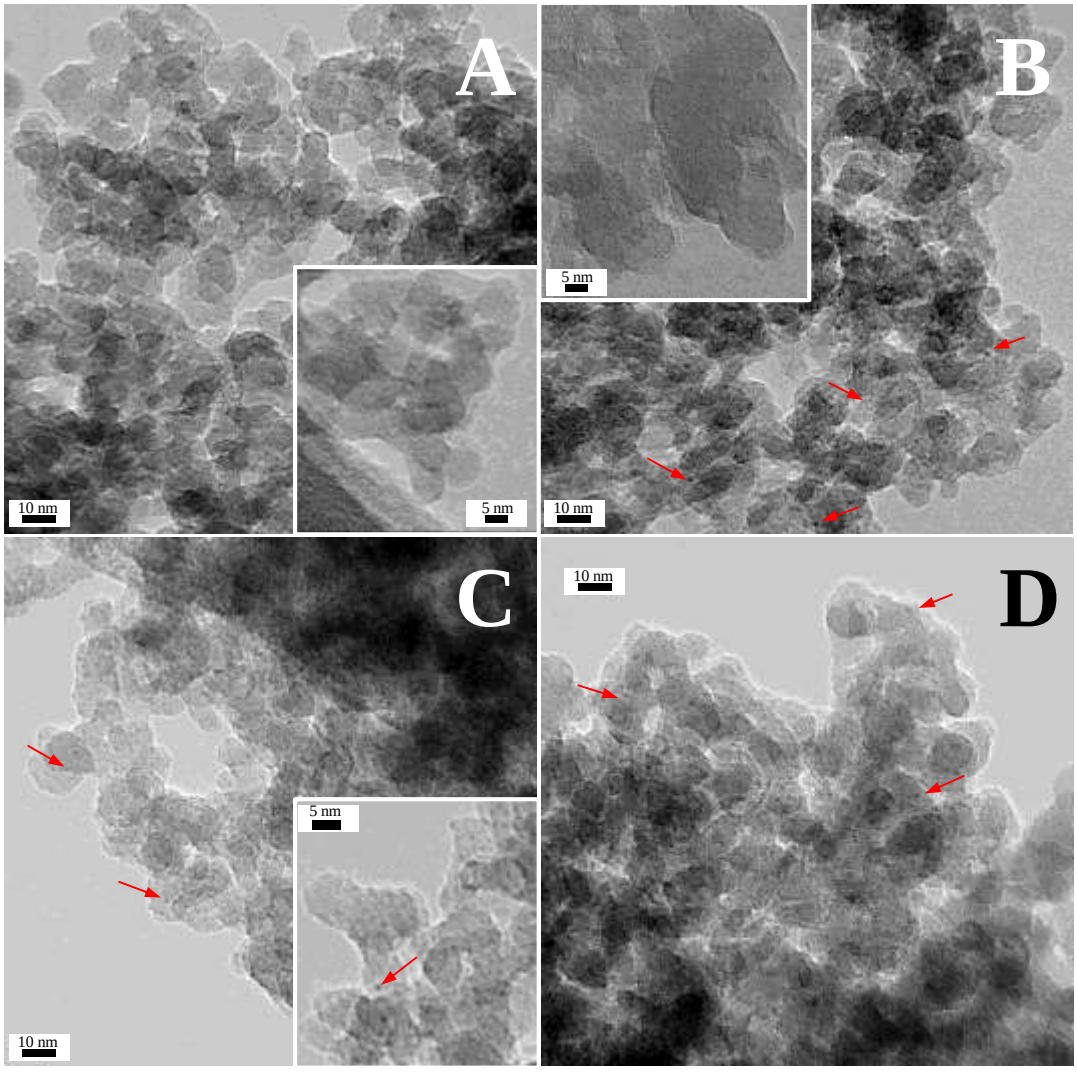

Fig. 2. TEM images of the fresh catalysts prepared in this work. Samples; A) $Fe_{0.005}SiO_2$, B), $Fe_{0.01}SiO_2$, C) $Fe_{0.03}SiO_2$ and D) $Fe_{impreg}SiO_2$.

The silica support obtained in this work has an amorphous structure without any apparent crystalline order, as extracted from the iron containing silica micrographs (e.g. Fig. 2A). In all cases, iron has been detected by EDX (Fig. S3 bottom) regardless the iron loading in the sample. It must be highlighted that detection of iron in the samples was confirmed even for the sample sections shown in the inserts of Fig. 2A-C, some of which do not display any appreciable nanoparticles (specifically insets in Fig. 2A and 2B), which is indicative of the good dispersion of the iron species in the sample. However, some differences can also be observed. For the sol-gel catalysts with low Fe contents ($Fe_{0.01}SiO_2$), some Fe particles (probably corresponding to iron oxide) can be observed, with a particle size that is around 1 nm, indicated by the red arrows. For the catalyst with the highest Fe content (Fe/Si=0.03), these particles can also be observed in a higher concentration (Fig. 2C). So, by using the one-step synthesis procedure, most of the iron species can be incorporated into the silica structure as isolated Fe(III) species , as it was detected for the sample with the lowest iron loading. As the Fe/Si ratio increases, the iron is also incorporated to a significant degree as small iron containing superficial clusters and larger particles of iron oxide around 1 nm of diameter [44].

On the other hand, for the iron based catalyst prepared by impregnation, a good dispersion of the iron oxide has been achieved (Fig. 2D). Small particles of iron oxide can be observed, in this case with particle sizes between 1-2 nm.

Large particles of iron oxide were not detected in any of the samples. XRD analyses (results not shown) performed to evaluate the chemical state of Fe in the samples did not yield any significant peaks arising from any iron-containing phase due to the small size and the small iron loading of the samples.

3.2 Spectroscopic Analysis of $Fe_{0.0X}SiO_2$ and $Fe_{impreg}SiO_2$

The solid UV-VIS analyses of the catalysts are shown in Fig. 3.

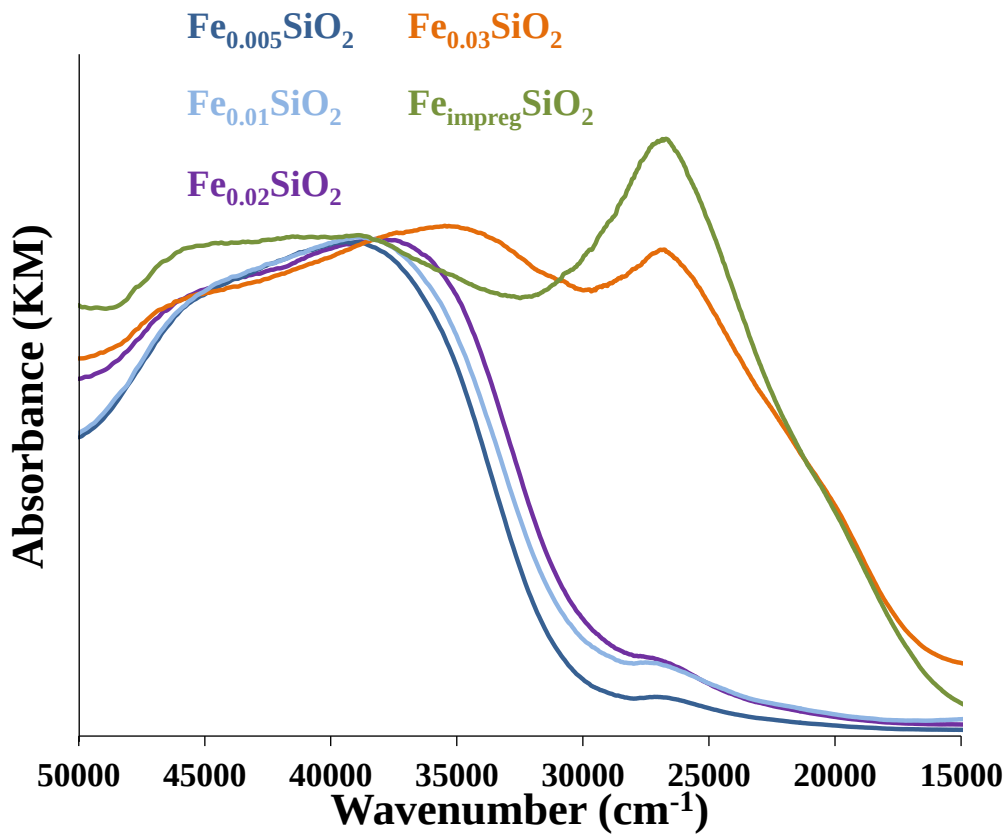

Fig. 3. Solid UV-VIS reflectance spectra of the fresh samples prepared in the work.

As it can be observed in Fig. 3, all the samples present significant UV-VIS radiation absorbance between 15000 and 50000 cm^{-1}, independently of the Fe content. In this sense, a commercial Fe_2O_3-bulk oxide (Sigma-Aldrich, Fig. S5) was also analyzed, presenting only two intense bands at 20000 and 25000 cm^{-1} and pure SiO_2 does not present any UV-VIS radiation absorption within the interval analyzed.

For the catalysts prepared in this work, important differences can be observed depending on the metal loading and the preparation method. In this sense, the samples prepared by one-step synthesis with Fe/Si ratios lower than 0.03, present a very weak signal at 27000 cm^{-1} (370 nm) and two intense bands at 38000 and 45000 cm^{-1} (260 and 220 nm, respectively). However, for the highest Fe/Si values ($Fe_{0.03}SiO_2$), the intensity of the peak at 27000 cm^{-1} is very similar to that of the bands at 38000 and 45000 cm^{-1}. This is also the case of the impregnated catalyst, where the band at 27000 cm^{-1} displays a higher intensity than the ones above 30000 cm^{-1}.

In addition, for these two catalysts ($Fe_{0.03}SiO_2$ and $Fe_{impreg}SiO_2$) with an intense band at 27000 cm^{-1}, a shoulder at around 20000 cm^{-1} (500 nm) can be observed in the spectra. Comparing the intensity of the 27000 cm^{-1} band for the catalysts prepared by the sol-gel route, it is possible to see that the intensity of this band depends on the Fe/Si ratio especially for loadings over 2 mol %. However, this effect is not observed for any of the other bands of the absorption spectra. It is very important to emphasize that both samples also show the corresponding UV-VIS bands attributed to isolated iron species (38000 and 45000 cm^{-1}) which are predominant in the sample with the lowest iron loading. Another important point is the difference between the $Fe_{impreg}SiO_2$ and commercial iron oxide (Fig. S5). For the impregnated sample the bands at 38000 and 45000 cm^{-1} can be clearly seen (with a relative intensity similar to that of the sample prepared by the sol-gel route) while these bands show a significantly lower intensity in the case of bulk Fe_2O_3.

Many studies have analyzed in depth the electronic transitions responsible for these absorption bands in this kind of materials and have identified different iron species supported on silica and/or well dispersed Fe species (such as single-site, di-iron sites or iron clusters) in inorganic materials [22,23,45,46]. Briefly, the authors conclude that large particles of iron oxide are responsible for the absorption between 20000-30000 cm^{-1}. In this sense, Fe_2O_3 particles present

an intense peak at 20000 cm^{-1}, FeO_x species shows a band at 23400 cm^{-1}, some aggregates of γ-FeOOH and $Fe(OH)_3$ display absorption at around 26000 cm^{-1} and finally Fe(III)-clusters present a band at 30000 cm^{-1} [23,45,46]. For the 30000-50000 cm^{-1} wavenumber interval, the pseudo-tetrahedral Fe(III) centers present a charge-transfer (CT) band at around 38000 cm^{-1} (the exact wavenumber depending on the solvent) and the same transition for octahedral iron complexes appears at 36000 cm^{-1} [23]. For a Fe(III) tetrahedral center, the molecular orbital theory predicts two intense transitions at 46500 and 41500 cm^{-1} corresponding to $t_1 \rightarrow t_2$ and $t_1 \rightarrow e$ transition electronic states, respectively. However, the octahedral Fe(III) centers also have two bands in the same wavenumber interval [46]. In this sense, all authors conclude that it is very complicated to unequivocally identify the coordination of the Fe(III) when it is very well dispersed over an inorganic support, like silica or a zeolite [46,47]. Recently, Prieto-Centurion et al. reported very well dispersed iron silica based on Fe-EDTA complex impregnation where the identification of the iron species was very exhaustive. Iron single-sites, small bi-dimensional iron superficial clusters and larger particles of iron oxide can be obtained modifying the iron precursor or the alkaline promotor [44].

In this sense, the interpretation of the UV-VIS spectra of iron based catalysts is not straightforward. In samples $Fe_{0.005}SiO_2$, $Fe_{0.01}SiO_2$ and $Fe_{0.02}SiO_2$, the presence of the weak band at 27000 cm^{-1} demonstrates that not all the iron of the sample is incorporated into the silica framework as well-dispersed species, despite of the intense bands at 38000 and 45000 cm^{-1} which are indicative of the iron being incorporated as well-dispersed species. The band at 27000 cm^{-1} increases slightly in intensity with increasing Fe content. However, considering the intensity of the band compared to the sample $Fe_{impreg}SiO_2$, we can conclude that most of the iron introduced to the synthesis solution is efficiently incorporated into the silica framework as

isolated iron. This is in agreement with the EDX results in the TEM analyses and FE-SEM observations (see Fig. S3), where the incorporation of iron prevented the formation of perfect µ-spheres of silica. The formation of some small iron superficial clusters and larger particles (around 1 nm) of iron oxide was also confirmed by TEM microscopy (Fig. 2) and is in good agreement with other related works based in alkaline-promoted iron catalysts [44]. It is quite difficult to quantify the fraction of iron which is well-dispersed and incorporated into the silica framework with respect to the rest of the iron oxide forming small particles.

E_g (bandgap energy) extracted by Kubelka-Munk analysis has demonstrated to be a very useful tool to investigate the dispersion of transition metals (Mo or Fe) over inorganic materials, such as silica or zeolites [26,48,49]. For example, the E_g values obtained for bulk α-Fe_2O_3 and nanoclusters of iron oxide in MCM-41 were 2.14 and 4.20 eV, respectively [49], and for well dispersed and KCl doped iron oxide over MFI zeolite around 4.50 eV [26]. The same authors [21] used XANES analysis and concluded that for samples with small Fe/Si ratios (0.01), the direct hydrothermal synthesis of an iron containing silica produces preferentially an iron incorporation in the tetrahedral framework positions obtaining similar values of E_g, around 4.20 eV, while other methodologies, such as ion-exchange or impregnation methods produce small iron oxides clusters with an octahedral coordination of the iron atoms.

Comparing the E_g energies obtained for the one-step synthesis catalysts in this work (which are 3.97, 3.91 and 3.90 eV for $Fe_{0.005}SiO_2$, $Fe_{0.01}SiO_2$ and $Fe_{0.02}SiO_2$, respectively) with other Fe-silicates values found in the literature, the results of this work are closer to those of well dispersed iron oxide on inorganic materials, such as silica or zeolites, were the E_g energies are around 4.20 eV, than to those of bulk iron oxide or large oxide particles [49]. On the contrary, for the sample $Fe_{0.03}SiO_2$, the intensity of the bands at 20000 and 27000 cm^{-1} suggests that the

iron species are mainly in the form of clusters and larger particles of iron oxide, with a calculated E_g for this sample of 2.51 eV, very close to bulk iron oxide [49]. However, these iron oxide particles are too small for XRD detection (results not shown).

For the $Fe_{impreg}SiO_2$ catalyst, the high absorbance of the sample at 20000 and 27000 cm^{-1} indicates that the iron oxide is preferentially deposited as small iron superficial clusters and larger particles over the silica surface. The bandgap value obtained in this case is 2.55 eV, which also indicates the formation these particles of iron oxide, as previously observed for the $Fe_{0.03}SiO_2$ catalyst.

The incorporation of the iron species into the silica framework can be also deduced by FTIR spectroscopy in the fresh catalysts after their drying at 120ºC for 24 h. The corresponding spectra are shown in Fig 4.

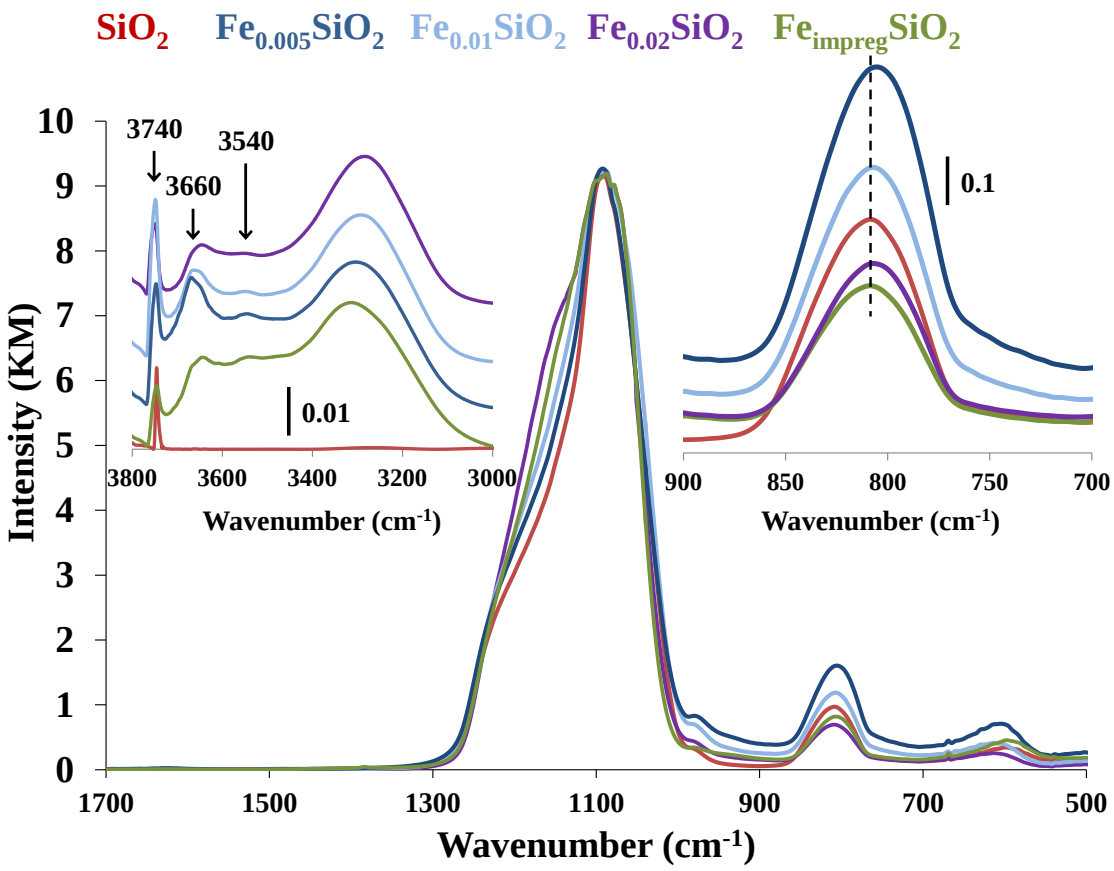

Fig. 4. FTIR spectra of the catalysts prepared in this work after drying at 120ºC for 24 h. The presented magnifications correspond to the OH (left) and SiO_4 (right) vibration regions.

Fig. 4 shows the IR spectra for the catalysts within the most relevant wavenumber ranges. The band located at 810 cm^{-1} corresponding to the asymmetric modes of the isolated [SiO_4] units is showed in the upper right corner in Fig. 4. This analysis shows that the maximum of the band (dotted line) is located at around 810 cm^{-1}, being this value obtained for the impregnated iron catalyst. However, for the one-step synthesis catalysts a small displacement to lower wavenumbers is observed (e.g. 804 cm^{-1} for the $Fe_{0.005}SiO_2$ catalyst). A similar effect was observed by Scarano et al. [50], where the presence of small amounts of heteroatoms was enough

to induce modifications in the framework stretching region. On the other hand, the most intense band located at 1090 cm^{-1}, corresponding to Si-O stretching, does not present any apparent modification. Bordiga et al. [46]described how the absorption of the [O_3Si-O] species surrounding the Fe(III) centers can emerge in a complex absorption band between 1250-1000 cm^{-1}. In this sense, it is quite difficult to differentiate this band due to the proximity of the fundamental framework modes of pure silica (1300-1000 cm^{-1}). However, as the iron loading increases a new shoulder appearing at approximately 1160 cm^{-1} increases its intensity (Fig. 4). This shoulder may appear as a consequence of the aforementioned complex band due to the increasing presence of iron species. It must be mentioned that it has been impossible to find the shoulder at 1006 cm^{-1}previously reported by the same work, corresponding to the framework Fe(III)-O stretching species, due to the calcination step applied to the samples, as they described in their work.

In the 2900 to 3800 cm^{-1} wavenumber region (top left corner of Fig. 4) it is possible to identify the OH stretching bands on the surface. Some bands can be detected and have been described in the literature [46,47,51]; isolated free silanol (3745 cm^{-1}), bridged hydroxyls with Brønsted acid character (3660 cm^{-1}) and H-bonded species in silanol (3500-3250 cm^{-1}). The raw silica presents only the band of the free silanol groups. However, when iron is incorporated the rest of the typical OH bands appear. It is very important to notice that the band corresponding to the bridged hydroxyls (3660 cm^{-1}) has a higher intensity in the case of $Fe_{0.005}SiO_2$ and decreases as the iron loading increases. On the other hand, the relative intensity of this band for the iron impregnated catalyst is very similar to the $Fe_{0.02}SiO_2$. This band presents a slight displacement to higher wavenumber values compared to similar materials (H-ZSM-5 (3610 cm^{-1}) and Fe-

Silicalite (3630 cm^{-1})). This higher wavenumber indicates a lower acid strength of the Brønsted bridged hydroxyls corresponding to the Si-OH-Fe species in the samples [46,47].

In this sense, the observation of the bridged hydroxyls and the displacement of the asymmetric modes of the isolated [SiO_4] due to the presence of iron may confirm the presence of Fe(III) species incorporated and well-dispersed into the silica framework, especially in the case of the lowest iron-content sample $Fe_{0.005}SiO_2$.

UV-Raman has been used as another complementary technique to determine the incorporation of iron into the silica framework in the fresh catalysts. The results are presented in the Fig. 5.

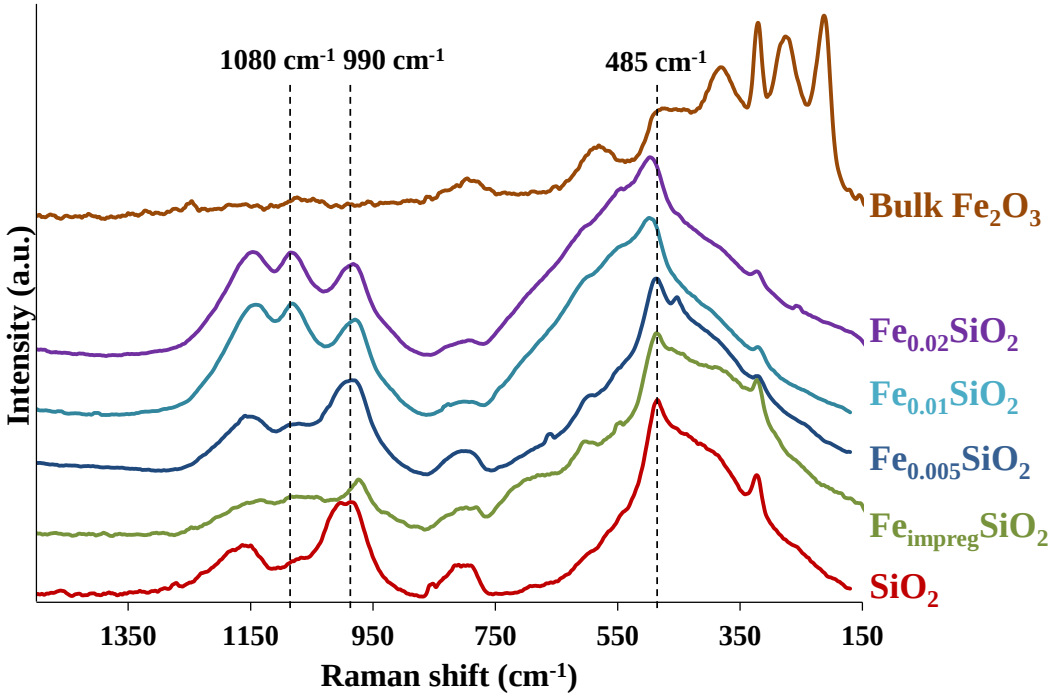

Fig. 5. UV resonance Raman spectra of the silica, fresh catalysts and pure Fe_2O_3 excited with a UV laser of 325 nm.

By UV-Raman it is possible to analyze the different coordination environments of the iron into crystalline aluminosilicates (such as ZSM-5) or amorphous silica materials (such as SBA-15) [52,53]. For the pure silica material the Raman bands of the symmetric and asymmetric Si-O-Si stretching appear at 485 and 990 cm^{-1}. These bands are not obtained for the commercial Fe_2O_3 material, which only presents a very intense Raman activity under 600 cm^{-1} due to its vibrational structure modes. For the iron based materials, three characteristics bands are reported for the amorphous silica materials. In their work (see Ref. [52]) at 510 and 1090 cm^{-1} the Fe-O-Si stretching modes of the Fe into the silica framework appear together with a band located at 978 cm^{-1} associated to the Si-O-Si vibrations near the iron species [52,53]. Two main features may be highlighted from Fig. 5. On the one hand, a blueshift displacement of the 485 cm^{-1} band is observed when the iron content increases in the one-step synthesis series (up to 500 cm^{-1} in the case of $Fe_{0.01}SiO_2$ and $Fe_{0.02}SiO_2$). For the $Fe_{impreg}SiO_2$ catalysts no modification of the Si-O-Si stretching band is observed, only the presence of a small band at 600 cm^{-1} which is also found in the bulk iron oxide. On the other hand, some modifications due to the presence of iron are observed in the 900-1200 cm^{-1} range. While there are no modifications in the 990 cm^{-1} band when iron is present in the synthesis, these are not conclusive and do not seem related to the amount of iron in the synthetic protocol. However, in the case of the band located at 1080 cm^{-1} a progressive increase in intensity is observed when the Fe/Si ratio increases up to a molar loading of 0.02.

Analyzing the results obtained by UV-Raman, and comparing with UV-VIS and FTIR, it is possible to confirm that iron is incorporated into the silica framework. Thus, with these results we have confirmed that as the iron loading increases in the one-step synthesis the silica framework is being modified by the presence of the incorporated iron species. Furthermore, for

the impregnated sample it is also possible to obtain an iron fraction of well-dispersed species. However, compared with the $Fe_{0.01}SiO_2$ catalysts, a higher amount of small particles/clusters of iron oxide is obtained.

In-situ FTIR has also been used to analyze the interaction between the components in the gas phase (propylene, molecular oxygen and gas stream reaction) and the catalysts, since this interaction is of importance to understand the performance of the catalyst in the propylene epoxidation reaction. The results corresponding to the $Fe_{0.005}SiO_2$ sample at 350ºC are presented in Fig. S6.

As it can be observed, after 5 minutes of interaction of the catalyst surface with the propylene stream, the gas is present on the ferrosilicate surface and therefore, intense CH_x symmetric and asymmetric stretching bands are observed in the spectrum at around 3000 cm^{-1}. Also, IR bands can be observed at around 1640 and 1840 cm^{-1}, corresponding to C=C stretching and of the molecular dipole moment parallel to the plane of symmetry vibrations, respectively [54]. In all cases, the IR signals correspond to those of pure propylene gas since no significant shift in the position of the peaks assigned to gaseous propylene [27,55] can be appreciated, which indicates that propylene is mostly physisorbed on the ferrosilicate surface. Stronger adsorbent-adsorbate interactions may not be ruled out altogether, but due to the low metal amount compared to the high concentration of adsorbed propylene the corresponding IR signals are inappreciable. When the gas stream is switched to pure He, a decrease in the intensity of the signals corresponding to physisorbed propylene can be gradually seen due to propylene desorption and, after 60 seconds, no evidence of propylene, or other hydrocarbon-related compound can be obtained and a flat IR spectrum is observed (red line). From these results, a weak interaction between propylene in the gas phase and the surface of the catalysts can be inferred at the reaction temperature. Similar

results have been obtained for the rest of the catalysts in this work and for the different temperatures tested, which have not been shown for the sake of brevity. Regarding the results of the O_2 desorption experiments, no results could be obtained due to the lack of IR signal from the molecular O_2. When the reaction mixture was flowed over the catalyst at 350ºC during the in situ FTIR analysis, no bands corresponding to propylene oxide molecule could be observed due to the small production of PO with respect to the propylene concentration. For the two analyzed samples (those with a 0.5% and 3% mol loading, see Fig. S6B), the catalyst with the higher activity ($Fe_{0.03}SiO_2$) showed a marked increase in the amount of generated water, as evidenced by the signals in the fingerprint region (1500-2000 cm^{-1}), as compared to the $Fe_{0.005}SiO_2$ sample. The presence of these bands together with the comparatively low PO production did not allow for the detection of the desired reaction product by in situ FTIR analysis. When the reaction was stopped (by flowing Helium through the reaction chamber), the spectrum returned to the initial appearance of the original catalyst.

3.3 Propylene Epoxidation Reaction

From the non-isothermal experiments, it is observed that the reaction starts (PO generation) in all cases at around 300ºC, reaching the maximum activity at around 400ºC. The PO selectivity in these tests is very stable throughout the entire temperature interval and, in general, shows slightly higher values at low conversions and tends to decrease as the activity increases (e.g. 27% at 320ºC versus 20% at 450ºC for the $Fe_{0.01}SiO_2$ sample).

After these preliminary experiments, the fresh samples were tested under isothermal conditions (at 350ºC) during at least 4 hours in two cycles. In all catalytic tests, the propylene conversion,

PO generation and PO selectivity remained constant for all the reaction time, and the values showed in this section correspond to the steady state conditions. Analyzing the other compounds produced in the reaction, it was possible to find out that the main byproduct formed was CO_2, but in some catalysts acetaldehyde, ethanol and acetone were also produced to a negligible extent (maximum selectivity for any of the products was always below 1%).

The results of the catalytic activity of the samples under steady-state conditions at 350ºC are shown in Table 1.

Table 1. Catalytic performance of the samples prepared in propylene epoxidation by O_2 molecule under steady-state conditions at 350ºC

Catalyst	C_3H_6 Conversion (%)	PO Generation (%)	Selectivity (%)			TOF (h^{-1})
			PO	Others[a]	CO_2	
1st Cycle						
$Fe_{0.005}SiO_2$	5.5	1.8	33.6	< 0.5	~66	10.8
$Fe_{0.01}SiO_2$	7.8	1.9	24.6	< 0.5	~75	4.8
$Fe_{0.02}SiO_2$	10.3	2.4	23.1	< 1.0	~76	3.6
$Fe_{0.03}SiO_2$	15.4	3.0	19.5	< 1.0	~80	2.7
$Fe_{impreg}SiO_2$	5.4	1.2	22.9	< 1.0	~76	3.5
2nd Cycle						
$Fe_{0.005}SiO_2$	5.6	1.9	33.3	< 0.5	~66	10.7
$Fe_{0.01}SiO_2$	6.0	1.4	23.5	< 0.5	~76	3.5
$Fe_{impreg}SiO_2$	4.7	1.1	22.8	< 1.0	~76	2.6

[a] Acetaldehyde is the main organic byproduct obtained in the catalytic reaction (always with a selectivity below 1%).

According to the results shown in Table 1, the catalytic results for the propylene epoxidation in O_2 atmosphere show that all the catalysts of this work are active in the studied reaction. As it can be observed, the propylene conversion gradually increases as the Fe/Si increases. For the sample with the lowest Fe/Si ratio, 5.5% of propylene conversion is obtained, while for the $Fe_{0.03}SiO_2$ catalyst the propylene conversion increases up to 15.4%. The PO generation presents the same trend, and also increases proportionally to the metal loading, showing for the abovementioned catalysts PO generation values of 1.8 and 3%, respectively. On the contrary, the opposite behavior is obtained for the selectivity, since it decreases as the iron metal loading increases, obtaining 33.6% of selectivity towards PO for the $Fe_{0.005}SiO_2$ sample versus a 19.5% in $Fe_{0.03}SiO_2$. If we analyze these results in terms of TOF, we can see that the sample with the lowest iron loading ($Fe_{0.005}SiO_2$) is the one with the highest TOF and, as the Fe/Si ratio increases, TOF values decrease and similar data are obtained for samples $Fe_{0.02}SiO_2$ and $Fe_{0.03}SiO_2$.

Regarding the samples with similar Fe/Si ratios but prepared using different methodologies, $Fe_{0.01}SiO_2$ and $Fe_{impreg}SiO_2$, the catalytic results observed were slightly different. $Fe_{0.01}SiO_2$ catalyst presents a 7.8% of propylene conversion versus 5.4% for $Fe_{impreg}SiO_2$. The PO selectivity also presents similar differences, with values of 24.6% for the one-step synthesis and 22.9%, for the impregnated catalyst. From these results, it can be extracted that the sol-gel synthesis yields catalysts with better properties for this epoxidation process than the impregnation procedure, as shown in Table 1 at 350ºC. The $Fe_{impreg}SiO_2$ catalyst shows a propylene conversion value similar to the $Fe_{0.005}SiO_2$ catalyst and the lowest PO generation for all the studied catalysts. The different catalytic behavior of the impregnated sample can be attributed to the broad and complex distribution of iron species on the silica support. The results corresponding to the one-step synthesis seem to indicate that not all the iron species contained in

the catalysts are equally active for the epoxidation reaction since, would that be the case, TOF values would be similar for all samples. However, the iron species in the $Fe_{0.005}SiO_2$ catalyst seem to be more active than those present on the catalysts with higher Fe contents. It should also be taken into account that propylene conversion increases significantly as the Fe content in the sample increases. Thus, in order to understand these two effects, we need to consider the results obtained by the experimental techniques applied (FE-SEM, TEM, FTIR, UV-Raman and UV-VIS) to the $Fe_{0.0X}SiO_2$ catalysts. These results suggest that it is possible to differentiate between two kind of iron species in the catalyst; i.e., well dispersed iron into the silica framework or superficial iron atoms in either tetrahedral or pseudo-tetrahedral coordination (mainly present in $Fe_{0.005}SiO_2$ catalyst, as detected by EDX and UV-VIS) and small iron superficial clusters and larger particles of iron oxide (around 1 nm in size) over the silica surface (present in the samples with high iron loadings). Thus, our hypothesis after the catalysts characterization is that as iron loading increases in the catalysts for the one-step synthesis, there is a higher fraction of iron species present as iron oxide clusters relative to the incorporated ones. In this sense, even for the samples with 3 mol % Fe prepared by the sol-gel route or even the impregnated samples analyzed with UV-Vis analyses, it is not possible to rule out the presence of a fraction of well-dispersed iron species incorporated in the silica framework (Fig. 3). On the other hand, as it can be seen in Fig. S5, there are noticeable differences in the UV-VIS spectra of the impregnated catalyst with respect to bulk iron oxide which may be attributed to the presence of well-dispersed iron species present in the sample, which may account for its observed catalytic activity. In case of the commercial iron oxide, the bands at 38000 and 45000 cm^{-1}, corresponding to isolated iron species present a very weak intensity (See Figure S5), while their relative intensities for the $Fe_{impreg}SiO_2$ catalysts are significantly larger. So from our results we can conclude that that the

iron species incorporated into the silica framework have a higher activity for PO generation versus the small particles of iron oxide, which are more active in the propylene conversion to CO_2 (i.e. total oxidation). Our hypothesis is in good agreement with the samples characterization and the obtained catalytic results.

To study the behavior of the samples after the first catalytic test, the samples were treated at 550ºC in air to remove any possible carbonaceous deposit and were then studied in subsequent cycles. The most representative catalytic activity results are presented in Table 1. Between each cycle, the samples were analyzed by solid UV-VIS spectroscopy.

The performance of these catalysts in terms of TOF for the two consecutive reaction cycles is presented in Table 1. It is possible to see the differences between the two cycles in the catalysts with a Fe/Si ration over 0.01, where a significant TOF decrease is observed for both the sol-gel catalysts and the iron-impregnated silica. The only exception to this observation is the $Fe_{0.005}SiO_2$ catalyst which presents the same value of TOF over the two catalytic cycles.

As it can be observed, a similar behavior is obtained for the catalysts in the two cycles. In this sense, the TOF drastically diminishes as the Fe content increases in the samples and, as a general trend, the second reaction cycle displays lower TOF values than the first cycle for all the catalysts, with the only exception of the $Fe_{0.005}SiO_2$ sample. In addition, in both cycles the impregnated sample (Table 1) shows the smallest TOF value. The catalytic performance of the $Fe_{0.005}SiO_2$ sample the propylene conversion remains constant 5.5%, and also the PO generation and the selectivity towards PO in the second cycle. However, for both samples with 1 mol % Fe, a poorer catalytic activity is obtained in the second cycle, diminishing both propylene conversion

and PO generation. As previously mentioned, the impregnated catalyst displays a poorer performance in terms of activity and selectivity compared to the corresponding sol-gel catalyst.

These results are in good agreement with the hypothesis that the species responsible for the catalytic epoxidation of propylene are the well dispersed iron atoms (isolated Fe(III) ions in tetrahedral or pseudo-tetrahedral coordination) into the silica framework. The sample with the lowest number of small iron oxide particles (around 1 nm) according to UV-VIS and TEM analysis and with the highest amount of iron incorporated in the silica structure is the $Fe_{0.005}SiO_2$ catalyst, and in this sense, this iron distribution is less liable to changes during the first epoxidation reaction cycle, as it was inferred from the TOF results. On the other hand, the samples with higher Fe/Si ratios present a higher amount of small iron superficial clusters and larger particles of iron oxide, as $Fe_{0.01}SiO_2$ and $Fe_{impreg}SiO_2$ catalysts, which are less active in propylene epoxidation with molecular O_2, and some changes might have occurred during the first catalytic cycle that might even affect to the iron species incorporated in the silica structure, reflecting in a poorer catalytic behavior in the second cycle. These results are in good agreement with other similar reported catalysts [44].

After each catalytic cycle, the samples were calcined at 550ºC in air and analyzed by UV-VIS spectroscopy (see Fig. S7 in Supplementary Information). As a result of the UV-VIS analyses when the catalysts were submitted to a catalytic epoxidation test the band located at 27000 cm^{-1} increases its intensity, with the only exception of the $Fe_{0.005}SiO_2$ sample which showed a negligible increase. The rest of the features of the spectra (bands at ~20000, 38000 and 45000 cm^{-1}) do not present any significant change after the reaction cycles. The modification of the intensity of this band suggests a modification of the E_g values obtained for the catalysts after the epoxidation reaction. Thus, for sample $Fe_{0.01}SiO_2$ the E_g value decreases from 3.91 (in the fresh

sample) to 3.80 eV in the used one. The samples have been analyzed by TEM after the propylene epoxidation test and no significant changes have been observed in the size and/or morphology of the iron oxide particles. However, the E_g value obtained after the epoxidation test for the $Fe_{0.005}SiO_2$ sample, 3.95 eV, does not differ significantly from that of the fresh catalyst. According to the catalytic reaction and the UV-VIS results, it seems that the E_g value is directly related to the catalytic performance of the Fe-doped catalysts and, in this sense, it seems that a decrease in the E_g parameter after the reaction (as it is the case of $Fe_{0.01}SiO_2$ and $Fe_{impreg}SiO_2$) reflects in a poorer performance of the catalysts, both in terms of propylene conversion and PO generation.

The slight decrease of the E_g values and the apparent impoverishment of the catalytic behavior (in terms of propylene conversion and TOF) for the catalysts with Fe content over 1 mol %, could be attributed to displacement/extraction of the iron species incorporated in the silica structure to extra-framework positions under reaction conditions (forming iron oxide deposited over the silica surface) or to a direct interaction with iron oxide nanoparticles, which would be less active in the propylene epoxidation reaction. This fact is observed in all samples, except for the lowest iron loading ($Fe_{0.005}SiO_2$), where the same TOF and propylene conversion have been obtained for the different cycles.

When critically comparing the results obtained in this work with those present in the literature, higher selectivity values (around 90%) can be found in other related works in gas-phase conditions, such as Au/Ti-SiO_2 catalyst in H_2/O_2 gas streams compositions, but in these catalysts lower propylene conversion are obtained [7,56,57]. On the other hand, the catalyst based on alkaline salts (K^+ or Na^+) doped iron silica require very powerful oxidizing agents, such as N_2O (without the presence of H_2 in the gas stream), to achieve PO selectivities around 60% for

propylene conversions below 10% [26,58]. In other cases the use of O_2 molecule as sole oxidant agent requires the use of more reactive metal oxides (Cu, Ru, Mo, Mn and/or W) to achieve the synthesis of the propylene oxide [14,16,18,59]. For example, Zheng et al. [60] have studied very interesting catalysts based in Ag-Cu nanoparticles deposited over $BaSO_4$ achieving a PO selectivity around 55% keeping a 3.6% of propylene conversion and Horváth et al. [61] have developed a pure MoO_x nanofilms over SiO_2 which present a PO yield around 2-3%, at least during 8 hours. In this regard, our catalyst show similar PO generation and slightly lower selectivities to PO only using a small amount of iron. As thoroughly summarised by Khatib and Oyama in a recent review [3], there are many examples in the literature in which molecular oxygen is used as the sole oxidant in the production of epoxides. This review clearly identifies three main catalysts groups (Ag-, Cu-, and Ti-based catalysts) with a fourth group ("Other types of catalysts" according to the authors) in which Au- and Mo-based catalysts seem promising alternatives. In terms of TOF, our systems show values over 10 h^{-1} which compare to some Ag-based systems [13], but would be below the data reported by Lei *et al*. [62] It must be noted, however, that mass spectrometry was used to analyze the reaction products which raises some questions concerning the selectivity of the prepared systems. The use of Cu-based systems, on the other hand has resulted in comparatively poorer TOF values [63]. In terms of conversion and selectivity, Cu-based catalysts seem to perform similarly to our systems (see for example) but the reported systems contain a significant loading of Ruthenium oxide, which is comparatively expensive. On the other hand, recent reports on Ag- and Ti-based systems have shown significantly higher selectivity (around 70-80%) [59] or conversion values (up to 97%) [64], even though the prepared catalysts are reasonably more sophisticated than those presented in this study. In any case, as it can be immediately seen from Fig. 7 in [3], the preparation of an

epoxidation catalyst which meets the current industrial demands requires the adequate balance between propylene conversion and yield towards its oxide. In our work, we present a simple preparation methodology to obtain iron based catalysts for propylene epoxidation using only O_2 molecules in the gas stream composition as oxidant, with conversion values above those obtained in some cases in the literature and good TOF values. The use of small quantities of an abundant and cheap metal, such as iron, well dispersed in the silica framework, allows for the simple preparation of a very user-friendly catalyst under the used reaction conditions. It should be noted that the obtained catalytic results are still distant from the objectives set in order to make these systems interesting from an applied point of view. However, these catalysts can be used as model to understand the epoxidation reaction pathway and, furthermore constitute a solid foundation from where these systems may be improved further in order to meet the industrial requirements in the future. On the other hand the TOF value obtained for the most selective sample in this work ($Fe_{0.005}SiO_2$, $10.8h^{-1}$) is significantly higher than that obtained for similar unpromoted catalysts found in the literature for the epoxidation reaction with N_2O [26], and slightly higher than those found for vanadium oxide based silica catalysts [27] and controlled copper oxide (Cu_2O) morphology [15]. The values of this work are similar to those presented by K-promoted copper oxide in different experimental conditions [65], although not as high as those obtained for certain gold based Ti-SiO_2 materials [66] although these studies use H_2/O_2 mixtures for the generation of oxidant peroxide species. It must be once again highlighted that the catalysts prepared in this study use dioxygen as the sole oxidant, which is an advantage over the oxidants employed in other reports, which either use more aggressive and/or toxic oxidants (N_2O, Cl_2 or H_2O_2) or gaseous mixtures containing explosive gases (H_2/O_2).

3.4 Results on computational calculations

Fe in the original cluster arranges itself in a pseudotetrahedral geometry as other authors have reported for the case of iron containing zeolites [42]. This proposed structure could correspond to the isolated Fe(III) ions incorporated into the silica framework in our hypothesis, specially in the sample with lowest amount of iron $Fe_{0.005}SiO_2$ where no small particles of iron oxide have been found. When O_2 interacts with the cluster, dioxygen incorporates to the structure coordinating itself to the Fe in a bridge mode slightly distorting the initial geometry and forming what will be referred as O_2-cluster complex (Fig. 6). It must be mentioned that the band at 38000 cm^{-1} in UV-VIS spectra (presented in our samples, see Fig. 3) has been previously assigned to pseudo-tetrahedral Fe(III) centers [23].

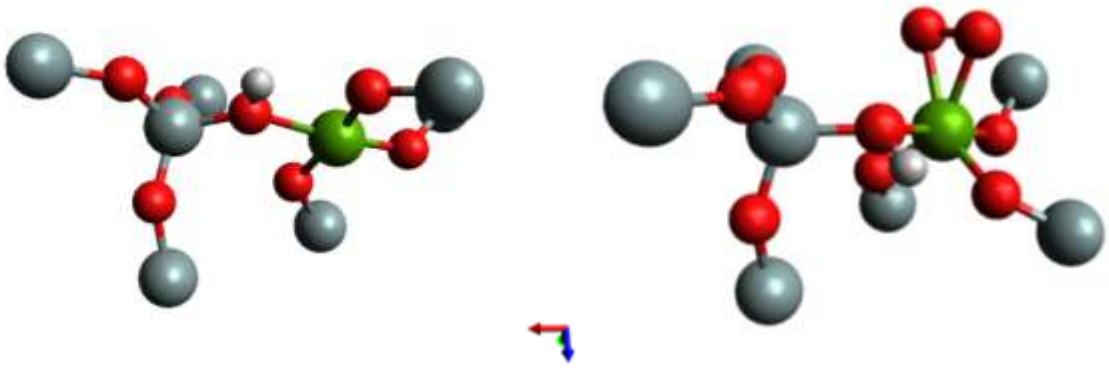

Fig. 6. Optimized simulated ferrosilicate clusters used in this study. Left: Original cluster; Right: O_2-cluster complex. Colour coding; Green: Iron; Red: Oxygen; Grey: Silicon; White: Hydrogen. Please note that only the acidic proton neighboring the Iron atom is represented for simplicity

Propylene adsorption has been modelled starting from different initial conditions: a direct interaction between propylene and iron and an interaction between propylene and the acid proton, see FTIR spectra at 3660 cm^{-1} in Fig. 4, (Fig. 7), as suggested by Nguyen et al for alkene adsorption on Al-zeolites [67].

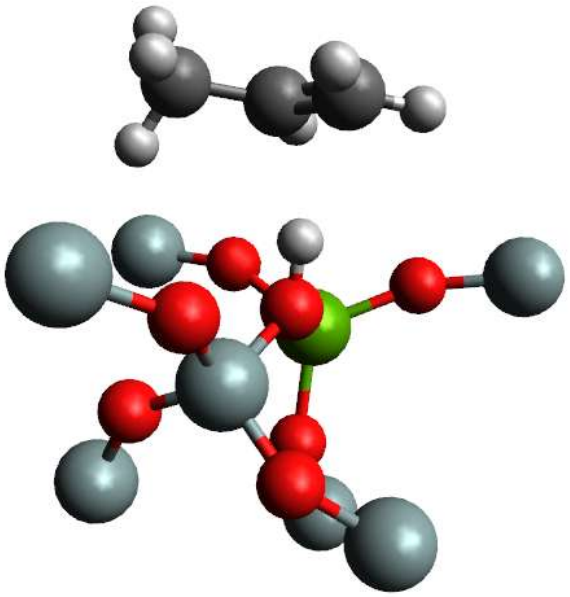

Fig. 7. Most stable optimized C_3H_6-cluster complex with the C_3H_6 in a bridge configuration over the acidic proton. Please note that only the acidic proton neighboring the Iron atom is represented for simplicity

Different multiplicities of the adsorbate-cluster complexes were studied as this can be important in the case of iron containing species [68,69]. Two different multiplicity situations were studied for the case of O_2-cluster complex: ferrosilicate cluster presents M=4 or M=6 and O_2-cluster complex M=2 or M=4 respectively. In this study the energetically most favorable combination of ferrosilicate cluster (M=4) and O_2-cluster complex (M=2) has been chosen for calculating the interaction energy.

For the case of propylene, the most stable C_3H_6-cluster complex is that in which the double bond interacts with the acidic proton of the ferrosilicate cluster (see Fig. 7). This configuration has been studied previously [67] and is in accordance with a precursor for the production of coke due to acid cracking reaction of the hydrocarbon. For this geometry, the most energetically stable cluster complex is the one where M=6 for both, the complex and the cluster.

Interaction energies for the most stable complexes have been obtained and presented in Table 2. These energy values are of the same order as those reported for alkene adsorption on different Al-zeolites [67].

Table 2. Calculated (B3LYP/6-31G(d,p)) interaction energies of the cluster-adsorbate complex

System	**E_{int} (eV)**
O_2-complex	0.434[a]
C_3H_6-complex	0.528[b]

[a] Energy corresponding to the interaction between the oxygen molecule and the single-site iron species
[b] Energy corresponding to the interaction between the propylene molecule and the acidic proton neighboring the iron species

Interaction energies between ferrosilicate cluster and the adsorbates (O_2 and C_3H_6) are quite similar, suggesting that both species interact with the surface to similar extents.

Table 3 presents selected bond distances of the adsorbates (O=O, C=C) both in the gas phase and adsorbed. A low increase in the bond distance of the adsorbates is observed as a result of activation of reactants upon adsorption on their respective adsorption sites.

Table 3. Calculated (B3LYP/6-31G(d,p)) bond distances of gas phase and adsorbed species (pseudotetrahedral iron atom for the O_2 molecule and acidic proton for the C_3H_6 molecule) .

System	Bond distance (Å)
d O=O in O_2 (gas phase)	**1.21**
d O=O in O_2 (cluster/O_2)	**1.29**
d C=C in C_3H_6 (gas phase)	**1.32**
d C=C in C_3H_6 (cluster/C_3H_6)	**1.34**

The interaction energy of both adsorbates with their corresponding adsorption sites is similarly small, showing that both compounds are weakly adsorbed. The calculated distances for the O=O and C=C bonds indicate that dioxygen is activated to a larger extent than propylene, which in turn makes the epoxidation possible in the ferrosilicate cluster shown in Fig. 6.

On the other hand, computational results also predict a significant interaction energy between propylene (π and σ complex) and the acidic proton located next to the single iron site. The slight difference in olefin bond distance in both interactions (with iron atom and acid proton for oxygen and propylene, respectively) would correspond to physisorbed species and is not enough to observe a IR-band displacement of the C=C in the sample $Fe_{0.005}SiO_2$ (Fig. S6A) maybe due to the small amount of iron present in the sample compared with the propylene concentration in the gas stream (see Fig. S6A). The interaction between the olefin and the acidic proton, is well known to produce cracking reactions and, in the presence of the activated oxygen in the neighbor position, could lead to either a partial or total oxidation of the hydrocarbon. These reactions (epoxidation, cracking and combustion) have been observed under the catalytic epoxidation conditions used in this work. From the results obtained in the epoxidation experiments, it becomes evident that the presence of well-dispersed iron species incorporated in the silicate

framework favours the preferential adsorption of oxygen over propylene, giving rise to an increase in the yield of the epoxide.

3.5 Discussion on the mechanism of epoxidation of propylene in the presence of dioxygen

The results obtained in this work together with those published for this and other reactions involving the activation of the O_2 molecule, enable us to propose a possible reaction pathway occurring on the ferrosilicate catalysts. In this sense, some works related to carbon monoxide oxidation on catalysts based on pure iron oxide or on inert supports need high temperatures for the reaction to take place (around 300ºC) [70,71]. In our case, propylene epoxidation on the highly dispersed iron species into the silica structure also begins under similar conditions. In addition, recent theoretical and experimental works have determined that the critical step for this reaction is the Fe-O formation of the terminal bond, that requires activation of the O=O bond [71,72]. This observation is in agreement with our computational calculations which postulate the interaction between isolated iron species and O_2, causing an increase in the O-O bond length of almost 7% which may react with the propylene adsorbed on the acidic proton located in its immediate vicinity. Also, the proposed mechanism for the propylene gas phase epoxidation over iron based catalyst with N_2O has been studied, and the authors propose that the iron catalyst activates the N_2O decomposition, and the atomic oxygen generated is the responsible for the propylene epoxidation [25].

With all this, and from the viewpoint of our work, it seems plausible that the well dispersed iron species incorporated into the silica skeleton of our system interact with molecular oxygen while the propylene molecule adsorbs on the neighboring acidic proton as the DFT calculations indicate. In the former case, the interaction between the well incorporated iron on the silica

structure and the O_2 molecule, produces the adsorption and activation of the gas molecule on the catalyst surface [73]. According to our evidence and the description proposed here, this process of propylene epoxidation with molecular oxygen over ferrosilicate catalysts would take place between the oxygen adsorbed on the well-dispersed iron species incorporated in the silica framework and the propylene adsorbed on the acidic proton to give the desired epoxide with significant efficiency under the reaction conditions. In this respect, the adsorption of propylene on the acidic proton favors the reaction of said compound with the activated oxygen molecule located in the isolated iron site, as we have also observed in our study. On the other hand, the interpretation of the dioxygen interaction with the surface with the small iron oxide cluster/particles, in some case lower than 1 nm, is very different depending on their size, atoms number and structure [74,75] and very difficult to construe in our catalyst. Furthermore, the existence (and the strength) of the acidic protons located next to the aforementioned clusters/particles would also play a role, which would further complicate the theoretical modelling of the system.

4. Conclusions

In this work we present a simple sol-gel methodology for the one-step synthesis of well dispersed iron sites in a silica framework in tetrahedral or pseudo-tetrahedral coordination and their application for the gas-phase epoxidation of propylene for the generation of propylene oxide only using O_2 molecule as oxidant reactant.

The synthetic procedure allows us to generate a user-friendly and cost-effective catalyst with different Fe sites depending on the Fe content, which range from pure single sites incorporated in

the silica matrix if the Fe content is low, to the formation of small particles of iron oxide (around 1 nm in size) when the Fe content is increased. In all cases, the catalysts are highly active and selective for the generation of PO, although our results seem to indicate that Fe species incorporated within the SiO_2 matrix have a higher activity towards the generation of the aimed product (PO). The active phases have proven to be modified under the reaction conditions, since several consecutive cycles show a decrease in both activity and selectivity towards PO when the iron content is over 1 mol %. In this sense, the distribution of isolated iron species into the silica framework presents a higher selectivity to PO production instead of the small iron superficial clusters and larger particles of iron oxide in catalysts whit higher metal loadings. O_2 activation by well-dispersed iron species over the silica structure is proposed to be responsible for the propylene epoxidation, and these active iron species could be moved to extra-framework positions after the first catalytic reaction in samples with Fe/Si ratios higher than 0.01 in both preparation procedure (one-step synthesis and impregnation based catalysts).

Simulation studies have identified that the presence of isolated iron species in tetrahedral or pseudo-tetrahedral coordination into the silica framework might be responsible for the adsorption of both molecular oxygen (only over isolated iron) and propylene (interacting with the acid proton), activating the former. This in turn enables the epoxidation of adsorbed propylene even in the absence of a noble metal catalyst, or even a catalyst in high loadings. In this sense, the prepared catalysts are still far from the thresholds with would qualify them for industrial application. However, the synthesis combined with the all the used techniques gives us a firm starting point from which to develop new catalysts and allows us to understand the catalytic process in order to improve the performance of the catalyst by their selective modification (e.g. adding some alkaline promoter to increase the PO selectivity) so as to meet industrial demands.

Finally, these catalysts prepared by one-step synthesis have proven to be more efficient for this process than a similar catalyst prepared by an impregnation procedure, where a poorer catalytic performance has been obtained.

Author information

Corresponding Author

*E-mail: a.berenguer@ua.es (Ángel Berenguer-Murcia)

Acknowledgments

We thank the MINECO, GV and FEDER (Projects CTQ2012-31762, CTQ2015-66080-R and PROMETEOII/2014/010) for financial support. A.B.M. and J.G.A. thank the Spanish Ministry of Economy and Competitiveness (MINECO) for their fellowships (RyC 2009-03913 and BES-2013-063678, respectively).

References

[1] D. Kahlich, U. Wiechern, J. Lindner, Propylene Oxide, Ullmann's Encycl. Ind. Chem. (2012) 313–335. doi:10.1002/14356007.a22.

[2] K. Singh, K. Merchant, Handbook of Industrial Chemistry and Biotechnology, in: Handb. Ind. Chem. Biotechnol., 2012: pp. 643–698. doi:10.1007/978-1-4614-4259-2.

[3] S.J. Khatib, S.T. Oyama, Direct Oxidation of Propylene to Propylene Oxide with Molecular Oxygen: A Review, Catal. Rev. 57 (2015) 306–344. doi:10.1080/01614940.2015.1041849.

[4] D. Trent, Propylene oxide, Kirk-Othmer Encycl. Chem. Technol. (2001) 1–26.

[5] T. Hayashi, K. Tanaka, M. Haruta, Selective Vapor-Phase Epoxidation of Propylene over Au/TiO2Catalysts in the Presence of Oxygen and Hydrogen, J. Catal. 178 (1998) 566–

575. doi:10.1006/jcat.1998.2157.

[6] X. Feng, X. Duan, H. Cheng, G. Qian, D. Chen, W. Yuan, et al., Au/TS-1 catalyst prepared by deposition–precipitation method for propene epoxidation with H2/O2: Insights into the effects of slurry aging time and Si/Ti molar ratio, J. Catal. 325 (2015) 128–135. doi:10.1016/j.jcat.2015.02.007.

[7] J. Huang, M. Haruta, Gas-phase propene epoxidation over coinage metal catalysts, Res. Chem. Intermed. 38 (2012) 1–24. doi:10.1007/s11164-011-0424-6.

[8] T.A. Nijhuis, J. Chen, S.M.A. Kriescher, J.C. Schouten, The Direct Epoxidation of Propene in the Explosive Regime in a Microreactor—A Study into the Reaction Kinetics, Ind. Eng. Chem. Res. 49 (2010) 10479–10485. doi:10.1021/ie1004306.

[9] E. Kertalli, D.M. Perez Ferrandez, J.C. Schouten, T.A. Nijhuis, Direct Synthesis of Propene Oxide from Propene, Hydrogen and Oxygen in a Catalytic Membrane Reactor, Ind. Eng. Chem. Res. 53 (2014) 16275–16284. doi:10.1021/ie502576n.

[10] V.I. Sobolev, K.Y. Koltunov, Catalytic epoxidation of propylene with CO/O2 over Au/TiO2, Appl. Catal. A Gen. 476 (2014) 197–203. doi:10.1016/j.apcata.2014.02.036.

[11] A. de Oliveira, A. Wolf, F. Schüth, Highly selective propene epoxidation with hydrogen/oxygen mixtures over titania-supported silver catalysts, Catal. Letters. 73 (2001) 157–160.

[12] A. Prieto, M. Palomino, U. Díaz, A. Corma, Propylene epoxidation with in situ generated H2O2 in supercritical conditions, Catal. Today. 227 (2014) 87–95. doi:10.1016/j.cattod.2013.10.004.

[13] J. Lu, J.J. Bravo-Suárez, M. Haruta, S.T. Oyama, Direct propylene epoxidation over modified Ag/CaCO3 catalysts, Appl. Catal. A Gen. 302 (2006) 283–295. doi:10.1016/j.apcata.2006.01.023.

[14] G. Jin, G. Lu, Y. Guo, Y. Guo, J. Wang, W. Kong, et al., Effect of preparation condition on performance of Ag-MoO3/ZrO2 catalyst for direct epoxidation of propylene by molecular oxygen, J. Mol. Catal. A Chem. 232 (2005) 165–172. doi:10.1016/j.molcata.2005.01.040.

[15] Q. Hua, T. Cao, X.-K. Gu, J. Lu, Z. Jiang, X. Pan, et al., Crystal-plane-controlled selectivity of Cu2O catalysts in propylene oxidation with molecular oxygen, Angew. Chem. Int. Ed. Engl. 53 (2014) 4856–61. doi:10.1002/anie.201402374.

[16] Ş. Kalyoncu, D. Düzenli, I. Onal, A. Seubsai, D. Noon, S. Senkan, Direct epoxidation of propylene to propylene oxide on various catalytic systems: A combinatorial micro-reactor study, Catal. Commun. 61 (2015) 16–20. doi:10.1016/j.catcom.2014.12.002.

[17] J. He, Q. Zhai, Q. Zhang, W. Deng, Y. Wang, Active site and reaction mechanism for the epoxidation of propylene by oxygen over CuOx/SiO2 catalysts with and without Cs + modification, J. Catal. 299 (2013) 53–66. doi:10.1016/j.jcat.2012.11.032.

[18] A. Seubsai, M. Kahn, B. Zohour, D. Noon, M. Charoenpanich, S. Senkan, Copper–Manganese Mixed Metal Oxide Catalysts for the Direct Epoxidation of Propylene by Molecular Oxygen, Ind. Eng. Chem. Res. 54 (2015) 2638–2645. doi:10.1021/ie5043598.

[19] Y. Lei, X. Chen, C. Xu, Z. Dai, K. Wei, Enhanced catalytic performance in the gas-phase

epoxidation of propylene over Ti-modified MoO3–Bi2SiO5/SiO2 catalysts, J. Catal. 321 (2015) 100–112. doi:10.1016/j.jcat.2014.10.015.

[20] Q. Zhu, R.M. Van Teeffelen, R.A. Van Santen, E.J.M. Hensen, Effect of high-temperature treatment on Fe/ZSM-5 prepared by chemical vapor deposition of FeCl3: II. Nitrous oxide decomposition, selective oxidation of benzene to phenol, and selective reduction of nitric oxide by isobutane, J. Catal. 221 (2004) 560–568. doi:10.1016/j.jcat.2003.09.025.

[21] Y. Wang, Q. Zhang, T. Shishido, K. Takehira, Characterizations of Iron-Containing MCM-41 and Its Catalytic Properties in Epoxidation of Styrene with Hydrogen Peroxide, J. Catal. 209 (2002) 186–196. doi:10.1006/jcat.2002.3607.

[22] A.W. Holland, G. Li, A.M. Shahin, G.J. Long, A.T. Bell, T.D. Tilley, New Fe/SiO2 materials prepared using diiron molecular precursors: Synthesis, characterization and catalysis, J. Catal. 235 (2005) 150–163. doi:10.1016/j.jcat.2005.07.003.

[23] C. Nozaki, C.G. Lugmair, A.T. Bell, T.D. Tilley, L. Berkeley, C. Road, Synthesis, Characterization, and Catalytic Performance of Single-Site Iron (III) Centers on the Surface of SBA-15 Silica, J. Am. Chem. Soc. (2002) 13194–13203.

[24] E. Ananieva, A. Reitzmann, Direct gas-phase epoxidation of propene with nitrous oxide over modified silica supported catalysts, Chem. Eng. Sci. 59 (2004) 5509–5517. doi:10.1016/j.ces.2004.09.006.

[25] B. Horváth, M. Šustek, I. Vávra, M. Mičušík, M. Gál, M. Hronec, Gas-phase epoxidation of propylene over iron-containing catalysts: the effect of iron incorporation in the support matrix, Catal. Sci. Technol. 4 (2014) 2664. doi:10.1039/c4cy00273c.

[26] Q. Zhang, Q. Guo, X. Wang, T. Shishido, Y. Wang, Iron-catalyzed propylene epoxidation by nitrous oxide: Toward understanding the nature of active iron sites with modified Fe-MFI and Fe-MCM-41 catalysts, J. Catal. 239 (2006) 105–116. doi:10.1016/j.jcat.2006.01.023.

[27] A. Held, J. Kowalska-Kuś, A. Łapiński, K. Nowińska, Vanadium species supported on inorganic oxides as catalysts for propene epoxidation in the presence of N2O as an oxidant, J. Catal. 306 (2013) 1–10. doi:10.1016/j.jcat.2013.06.001.

[28] G. Puy, C. Demesmay, J.L. Rocca, J. Iapichella, A. Galarneau, D. Brunel, Electrochromatographic behavior of silica monolithic capillaries of different skeleton sizes synthesized with a simplified and shortened sol-gel procedure., Electrophoresis. 27 (2006) 3971–80. doi:10.1002/elps.200600153.

[29] J. García-Aguilar, I. Miguel-García, A. Berenguer-Murcia, D. Cazorla-Amorós, Synthesis of Robust Hierarchical Silica Monoliths by Surface- Mediated Solution/Precipitation Reactions over Different Scales: Designing Capillary Microreactors for Environmental Applications, ACS Appl. Mater. Interfaces. 6 (2014) 22506–22518.

[30] M.J. Frisch, G.W. Trucks, H.B. Schlegel, G.E. Scuseria, M.A. Robb, J.R. Cheeseman, et al., Gaussian 09, Revision D. 01; Gaussian: Wallingford, CT, USA, 2009, (n.d.).

[31] A.D. Becke, Density-functional exchange-energy approximation with correct asymptotic behavior, Phys. Rev. A. 38 (1988) 3098–3100. doi:10.1103/PhysRevA.38.3098.

[32] C. Lee, W. Yang, R.G. Parr, Development of the Colle-Salvetti correlation-energy formula into a functional of the electron density, Phys. Rev. B. 37 (1988) 785–789.

doi:10.1103/PhysRevB.37.785.

[33] P.C. Hariharan, J.A. Pople, The influence of polarization functions on molecular orbital hydrogenation energies, Theor. Chim. Acta. 28 (1973) 213–222. doi:10.1007/BF00533485.

[34] M.M. Francl, W.J. Pietro, W.J. Hehre, J.S. Binkley, M.S. Gordon, D.J. DeFrees, et al., Self-consistent molecular orbital methods. XXIII. A polarization-type basis set for second-row elements, J. Chem. Phys. 77 (1982) 3654–3665. doi:10.1063/1.444267.

[35] V.A. Rassolov, J.A. Pople, M.A. Ratner, T.L. Windus, 6-31G∗ basis set for atoms K through Zn, J. Chem. Phys. 109 (1998) 1223. doi:10.1063/1.476673.

[36] S. Grimme, J. Antony, S. Ehrlich, H. Krieg, A consistent and accurate ab initio parametrization of density functional dispersion correction (DFT-D) for the 94 elements H-Pu, J. Chem. Phys. 132 (2010) 154104. doi:10.1063/1.3382344.

[37] S. Grimme, S. Ehrlich, L. Goerigk, Effect of the damping function in dispersion corrected density functional theory, J. Comput. Chem. 32 (2011) 1456–1465. doi:10.1002/jcc.21759.

[38] M.W. Wong, Vibrational frequency prediction using density functional theory, Chem. Phys. Lett. 256 (1996) 391–399.

[39] S. Boys, F. Bernardi, The calculation of small molecular interactions by the differences of separate total energies. Some procedures with reduced errors, Mol. Phys. (1970) 553–566. doi:10.1080/00268977000101561.

[40] F.B. van Duijneveldt, J.G.C.M. van Duijneveldt-van de Rijdt, J.H. van Lenthe, State of the Art in Counterpoise Theory, Chem. Rev. 94 (1994) 1873–1885. doi:10.1021/cr00031a007.

[41] M.D. Hanwell, D.E. Curtis, D.C. Lonie, T. Vandermeerschd, E. Zurek, G.R. Hutchison, Avogadro: An advanced semantic chemical editor, visualization, and analysis platform, J. Cheminform. 4 (2012) 1–17. doi:10.1186/1758-2946-4-17.

[42] M.S. Stavet, J.B. Nicholas, Density Functional Studies of Zeolites. 2. Structure and Acidity of [TI-ZSM-5 Models (T = B, Al, Ga, and Fe), J. Phys. Chem. 99 (1995) 15046–15061. doi:10.1021/j100041a021.

[43] Á. Berenguer-Murcia, D. Cazorla-Amorós, Á. Linares-Solano, MCM-41 Porosity: Are Surface Corrugations Micropores?, Adsorpt. Sci. Technol. 29 (2011) 443–455. doi:10.1260/0263-6174.29.5.443.

[44] D. Prieto-Centurion, A.M. Boston, J.M. Notestein, Structural and electronic promotion with alkali cations of silica-supported Fe(III) sites for alkane oxidation, J. Catal. 296 (2012) 77–85. doi:10.1016/j.jcat.2012.09.004.

[45] B. Heinrichs, L. Rebbouh, J.W. Geus, S. Lambert, H.C.L. Abbenhuis, F. Grandjean, et al., Iron(III) species dispersed in porous silica through sol-gel chemistry, J. Non. Cryst. Solids. 354 (2008) 665–672. doi:10.1016/j.jnoncrysol.2007.07.071.

[46] S. Bordiga, R. Buzzoni, F. Geobaldo, C. Lamberti, E. Giamello, A. Zecchina, et al., Structure and Reactivity of Framework and Extraframework Iron in Fe-Silicalite as Investigated by Spectroscopic and Physicochemical Methods, J. Catal. 158 (1996) 486–501. doi:10.1006/jcat.1996.0048.

[47] E.J.M. Hensen, Q. Zhu, M.M.R.M. Hendrix, A.R. Overweg, P.J. Kooyman, M. V. Sychev, et al., Effect of high-temperature treatment on Fe/ZSM-5 prepared by chemical vapor deposition of FeCl3: I. Physicochemical characterization, J. Catal. 221 (2004) 569–583. doi:10.1016/j.jcat.2003.09.024.

[48] M. Anpo, M. Matsuoka, Y. Shioya, H. Yamashita, E. Giamello, C. Morterra, et al., Preparation and characterization of the Cu+/ZSM-5 catalyst and its reaction with NO under UV irradiation at 275 K. In situ photoluminescence, EPR, and FT-IR investigations, J. Phys. Chem. 98 (1994) 5744–5750.

[49] M. Iwamoto, T. Abe, Y. Tachibana, Control of bandgap of iron oxide through its encapsulation into SiO2-based mesoporous materials, J. Mol. Catal. A Chem. 155 (2000) 143–153. doi:10.1016/S1381-1169(99)00330-1.

[50] D. Scarano, A. Zecchina, S. Bordiga, F. Geobaldo, G. Spoto, G. Petrini, et al., Fourier-transform infrared and Raman spectra of pure and Al-, B-, Ti- and Fe-substituted silicalites: stretching-mode region, J. Chem. Soc. Faraday Trans. 89 (1993) 4123. doi:10.1039/ft9938904123.

[51] J.P. Gallas, J.M. Goupil, A. Vimont, J.C. Lavalley, B. Gil, J.P. Gilson, et al., Quantification of water and silanol species on various silicas by coupling IR spectroscopy and in-situ thermogravimetry, Langmuir. 25 (2009) 5825–5834. doi:10.1021/la802688w.

[52] F. Fan, Z. Feng, C. Li, UV Raman Spectroscopic Studies on Active Sites and Synthesis Mechanisms of Transition Metal-Containing Microporous and Mesoporous Materials, Acc. Chem. Res. 43 (2010) 378–387. doi:10.1021/ar900210g.

[53] Y. Li, Z. Feng, H. Xin, F. Fan, J. Zhang, P.C.M.M. Magusin, et al., Effect of Aluminum on the Nature of the Iron Species in Fe-SBA-15, J. Phys. Chem. B. 110 (2006) 26114–26121. doi:10.1021/jp0657641.

[54] R.C. Lord, P. Venkateswarlu, The Infrared Spectra of Propylene and Propylene-d_6, J. Opt. Soc. Am. 43 (1953) 1079. doi:10.1364/JOSA.43.001079.

[55] A. Ruiz, B. van der Linden, M. Makkee, G. Mul, Acrylate and propoxy-groups: Contributors to deactivation of Au/TiO2 in the epoxidation of propene, J. Catal. 266 (2009) 286–290. doi:10.1016/j.jcat.2009.06.019.

[56] A.K. Sinha, S. Seelan, T. Akita, S. Tsubota, M. Haruta, Vapor phase propylene epoxidation over Au/Ti-MCM-41 catalysts prepared by different Ti incorporation modes, Appl. Catal. A Gen. 240 (2003) 243–252. doi:10.1016/S0926-860X(02)00451-9.

[57] B. Taylor, J. Lauterbach, W.N. Delgass, The effect of mesoporous scale defects on the activity of Au/TS-1 for the epoxidation of propylene, Catal. Today. 123 (2007) 50–58. doi:10.1016/j.cattod.2007.01.005.

[58] S. Yang, W. Zhu, Q. Zhang, Y. Wang, Iron-catalyzed propylene epoxidation by nitrous oxide: Effect of boron on structure and catalytic behavior of alkali metal ion-modified FeOx/SBA-15, J. Catal. 254 (2008) 251–262. doi:10.1016/j.jcat.2008.01.002.

[59] S. Ghosh, S.S. Acharyya, R. Tiwari, B. Sarkar, R.K. Singha, C. Pendem, et al., Selective Oxidation of Propylene to Propylene Oxide over Silver-Supported Tungsten Oxide Nanostructure with Molecular Oxygen, ACS Catal. 4 (2014) 2169–2174. doi:10.1021/cs5004454.

[60] X. Zheng, Q. Zhang, Y. Guo, W. Zhan, Y. Guo, Y. Wang, et al., Epoxidation of propylene by molecular oxygen over supported Ag-Cu bimetallic catalysts with low Ag loading, J. Mol. Catal. A Chem. 357 (2012) 106–111. doi:10.1016/j.molcata.2012.01.027.

[61] B. Horváth, M. Hronec, I. Vávra, M. Šustek, Z. Križanová, J. Dérer, et al., Direct gas-phase epoxidation of propylene over nanostructured molybdenum oxide film catalysts, Catal. Commun. 34 (2013) 16–21. doi:10.1016/j.catcom.2013.01.006.

[62] Y. Lei, F. Mehmood, S. Lee, J. Greeley, B. Lee, S. Seifert, et al., Increased Silver Activity for Direct Propylene Epoxidation via Subnanometer Size Effects, Science (80-.). 328 (2010) 224–228. doi:10.1126/science.1185200.

[63] O.P.H. Vaughan, G. Kyriakou, N. Macleod, M. Tikhov, R.M. Lambert, Copper as a selective catalyst for the epoxidation of propene, J. Catal. 236 (2005) 401–404. doi:10.1016/j.jcat.2005.10.019.

[64] K. Murata, Y. Kiyozumi, Oxidation of propene by molecular oxygen over Ti-modified silicalite catalysts, Chem. Commun. 2 (2001) 1356–1357. doi:10.1039/b101857o.

[65] Y. Wang, H. Chu, W. Zhu, Q. Zhang, Copper-based efficient catalysts for propylene epoxidation by molecular oxygen, Catal. Today. 131 (2008) 496–504. doi:10.1016/j.cattod.2007.10.022.

[66] N. Yap, Reactivity and stability of Au in and on TS-1 for epoxidation of propylene with H2 and O2, J. Catal. 226 (2004) 156–170. doi:10.1016/j.jcat.2004.05.016.

[67] C.M. Nguyen, B. a. De Moor, M.F. Reyniers, G.B. Marin, Physisorption and chemisorption of linear alkenes in zeolites: A combined QM-Pot(MP2//B3LYP:GULP)-statistical thermodynamics study, J. Phys. Chem. C. 115 (2011) 23831–23847. doi:10.1021/jp2067606.

[68] A. Heyden, N. Hansen, A.T. Bell, F.J. Keil, Nitrous oxide decomposition over Fe-ZSM-5 in the presence of nitric oxide: A comprehensive DFT study, J. Phys. Chem. B. 110 (2006) 17096–17114. doi:10.1021/jp062814t.

[69] S.P. Yuan, J.G. Wang, Y.W. Li, H. Jiao, Density functional investigations into the siting of Fe and the acidic properties of isomorphously substituted mordenite by B, Al, Ga and Fe, J. Mol. Struct. THEOCHEM. 674 (2004) 267–274. doi:http://dx.doi.org/10.1016/S0166-1280(03)00463-9.

[70] J.S. Walker, G.I. Straguzzi, W.H. Manogue, G.C.A. Schuit, Carbon Monoxide and Propene Oxidation by Iron Oxides for Auto-Emission Control, J. Catal. 110 (1988) 298–309.

[71] S. Royer, D. Duprez, Catalytic Oxidation of Carbon Monoxide over Transition Metal Oxides, ChemCatChem. 3 (2011) 24–65. doi:10.1002/cctc.201000378.

[72] W. Xue, Z.C. Wang, S.G. He, Y. Xie, E.R. Bernstein, Experimental and theoretical study of the reactions between small neutral iron oxide clusters and carbon monoxide., J. Am. Chem. Soc. 130 (2008) 15879–15888. doi:10.1021/ja8023093.

[73] M. V. Parfenov, E. V. Starokon, S. V. Semikolenov, G.I. Panov, O2 isotopic exchange in the presence of O- anion radicals on the FeZSM-5 surface, J. Catal. 263 (2009) 173–180. doi:10.1016/j.jcat.2009.02.009.

[74] D. Schroeder, A. Fiedler, J. Schwarz, H. Schwarz, Generation and Characterization of the Anionic, Neutral, and Cationic Iron-Dioxygen Adducts [FeO2] in the Gas Phase, Inorg. Chem. 33 (1994) 5094–5100. doi:10.1021/ic00100a039.

[75] L.-S. Wang, H. Wu, S.R. Desai, Sequential Oxygen Atom Chemisorption on Surfaces of Small Iron Clusters, Phys. Rev. Lett. 76 (1996) 4853–4856. doi:10.1103/PhysRevLett.76.4853.